

---

# Detecting Systematic Weaknesses in Vision Models along Predefined Human-Understandable Dimensions

**Sujan Sai Gannamaneni**  
*Fraunhofer IAIS, Lamarr Institute*

*sujan.sai.gannamaneni@iais.fraunhofer.de*

**Rohil Prakash Rao**  
*Fraunhofer IAIS*

*rohil.prakash.rao@iais.fraunhofer.de*

**Michael Mock**  
*Fraunhofer IAIS*

*michael.mock@iais.fraunhofer.de*

**Maram Akila**  
*Fraunhofer IAIS, Lamarr Institute*

*maram.akila@iais.fraunhofer.de*

**Stefan Wrobel**  
*Fraunhofer IAIS, University of Bonn*

*stefan.wrobel@iais.fraunhofer.de*

## Abstract

Studying systematic weaknesses of DNNs has gained prominence in the last few years with the rising focus on building safe AI systems. Slice discovery methods (SDMs) are prominent algorithmic approaches for finding such systematic weaknesses. They identify top-k semantically coherent slices/subsets of data where a DNN-under-test has low performance. For being directly useful, e.g., as evidences in a safety argumentation, slices should be aligned with human-understandable (safety-relevant) dimensions, which, for example, are defined by safety and domain experts as parts of the operational design domain (ODD). While straightforward for structured data, the lack of semantic metadata makes these investigations challenging for unstructured data. Therefore, we propose a complete workflow which combines contemporary foundation models with algorithms for combinatorial search that consider structured data and DNN errors for finding systematic weaknesses in images. In contrast to existing approaches, ours identifies weak slices that are in line with predefined human-understandable dimensions. As the workflow includes foundation models, its intermediate and final results may not always be exact. Therefore, we build into our workflow an approach to address the impact of noisy metadata. We evaluate our approach w.r.t. its quality on four popular computer vision datasets, including autonomous driving datasets like Cityscapes, BDD100k, and RailSem19, while using multiple state-of-the-art models as DNNs-under-test.

## 1 Introduction

With the recent advances in machine learning (ML), in particular, self-supervised techniques, there is a significant improvement in modelling of unstructured data like images. However, for safety-critical applications, ML models need to be developed with a focus on trustworthiness by investigating and correcting potential failure modes. To that end, systematic errors of the DNNs need to be studied and rectified. Hidden stratification (Oakden-Rayner et al., 2020) and fairness-related bias (Buolamwini & Gebru, 2018; Wang et al., 2020; Li et al., 2023) due to spurious correlations (Xiao et al., 2020; Geirhos et al., 2020; Mahmood et al., 2021) and underrepresented subpopulations (Santurkar et al., 2020; Sagawa et al., 2019) are some examples of a potential failure modes where the error or weakness is systematic in nature. The existence

---

of these modes implies that there are slices <sup>1</sup> of data where the performance of the DNN-under-test (**DuT**) is worse than the average performance on the entire test dataset. While identifying slices w.r.t. weak performance would be trivial by simply grouping samples on which models have high error, identifying slices that are both semantically coherent and have high error is challenging. This is due to the lack of semantic metadata describing the slices for many data domains (e.g., images, text). However, discovering semantically coherent weak slices is very beneficial and can be seen as a human-understandable global explanation of the model behavior. In addition, a semantically coherent weak slice is more actionable w.r.t. mitigation when debugging or auditing the models.

From a safety and certification perspective, upcoming standards (e.g., ISO/PAS 8800 (ISO, 2024)), and works with a focus on AI in automotive (Koopman & Fratrick, 2019; Burton et al., 2022), aerospace (EASA, 2023) and railway (Zeller et al., 2023) domains have highlighted the importance of data completeness and quality using, in most cases, Operational Design Domains (ODDs). In the KI-A Project <sup>2</sup>, Herrmann et al. (2022) have proposed ontologies for different traffic participants that can be used in building ODDs for automated driving. The goal of using such ODDs is to describe the scope of AI applications in terms of human-understandable, safety-relevant dimensions where comprehensible safety argumentations can be built w.r.t. robustness, explainability, interpretability, etc. To facilitate building such safety augmentations, testing approaches for ML developers and safety experts that evaluate DNN performance and identify systematic weaknesses are essential.

Although in recent years, several works (Chung et al., 2019; Sagadeeva & Boehm, 2021; d’Eon et al., 2022; Eyuboglu et al., 2022; Metzen et al., 2023; Plumb et al., 2023; Jain et al., 2023; Gao et al., 2023) have proposed methods for analysing systematic weaknesses, there is a lack of focus on identifying weaknesses of models evaluated on real-world datasets where the weaknesses align with human-understandable semantic concepts defined by, e.g., safety experts in ODDs. We argue that it is more beneficial from a safety perspective if the approaches to identify systematic weaknesses are ODD compliant for two main reasons: (i) the slices are **useful** as the identified vulnerabilities are aligned with human-understandable safety-relevant dimensions. (ii) the slices are **actionable** as ML developers can gather more data to retrain or reweigh the existing samples to improve performance along the safety-relevant dimensions. We address the challenge of analysing unstructured image data by designing a modular workflow that leverages recent advances in foundational models (Radford et al., 2021) and systematic weakness analysis methods for structured data (Sagadeeva & Boehm, 2021). Our contributions can be summarized as follows:

- We introduce a modular workflow that takes in an image dataset, ODD description and performance values of a **DuT** as inputs and outputs systematic weaknesses of the **DuT** (see section 3).
- Concretely, as part of the metadata generation module, we make use of CLIP (Radford et al., 2021) to leverage its rich joint image, text embedding space. As part of the slice discovery module, we propose using SliceLine (Sagadeeva & Boehm, 2021) with modifications to identify weak slices which align with the ODD (see section 3).
- In addition, we address the noisy nature of metadata generation and propose a method to recover relevant weak slices even if CLIP labelling is suboptimal. We empirically evaluate the behaviour of our workflow at various levels of labelling quality using synthetic data (see section 4).
- Furthermore, we evaluate DNNs trained and tested on real-world data, including three existing SOTA DNNs for autonomous driving and provide insights into their systematic weaknesses (see section 5.3).

## 2 Related Work

In this section, we discuss the recent progress in analysing systematic weakness using slice discovery methods (SDMs) (Eyuboglu et al., 2022) for structured and unstructured data and the relationship to interpretability and feature attribution methods.

---

<sup>1</sup>In literature, slices are often also called subgroups or subsets of data. All three terms are used interchangeably in relation to systematic weakness analysis.

<sup>2</sup><https://www.ki-absicherung-projekt.de/en/>

---

For structured data, works like SliceFinder (Chung et al., 2019) and SliceLine (Sagadeeva & Boehm, 2021) use the rich metadata available in the form of features to slice the data and exhaustively search for top-k low-performing slices. The differences between these two approaches occur in the scoring of the errors, the pruning strategy and how they deal with slice sizes. While these two approaches were explicitly developed for finding systematic weaknesses, subgroup-discovery techniques (Atzmueller, 2015), a subset of data mining, have a similar problem formulation and can also be potentially used for slice discovery of structured data.

For unstructured data like images, as metadata is not directly available, SOTA approaches have taken two lines of research. In the first line of prior work, for a given test dataset, DNN embeddings are used as proxies for coherency. Weak-performing slices of the data are obtained by clustering these embeddings along with model errors. Here, approaches like Spotlight (d’Eon et al., 2022) perform the clustering on the embeddings of the final layers of the **DuT** itself. In contrast, recent approaches leverage the joint embedding space of foundational models like CLIP (Radford et al., 2021) and apply mixture models (Eyuboglu et al., 2022) or SVMs (Jain et al., 2023) to identify coherent clusters. In (d’Eon et al., 2022), an additional step involving humans is required to inspect and understand what uniquely constitutes a weak slice. Approaches (Eyuboglu et al., 2022; Jain et al., 2023) automate the slice description process to reduce human effort and bias using an additional DNN. In all these approaches, as coherence is only loosely enforced based on DNN embeddings, it is not always clear what specific human-understandable concept uniquely constitutes a slice. Without this knowledge, it would be unclear to the ML developers what new data samples would need to be collected to retrain the model and fix the systematic weakness. As a mitigation to this problem, some approaches (Gao et al., 2023; Slyman et al., 2023) propose iterative human-in-the-loop testing to ensure that the identified slices are human-understandable.

In the second line of prior work, inspired by counterfactuals and leveraging CLIP, several approaches (Wiles et al., 2022; Metzen et al., 2023) propose synthetically generating new (counterfactual) images that would lead to erroneous predictions by controlling the content and the data shift in the image. Among those, PromptAttack (Metzen et al., 2023) also proposes to identify weaknesses that are aligned with the ODDs. However, while PromptAttack generates new samples using image-generation DNNs, which could potentially introduce biases due to domain shift, our approach is more aligned with earlier approaches that evaluate a DNN on a given test dataset. In this direction, HiBug (Chen et al., 2023) utilizes a GPT based model to assign attributes to a given dataset. In continuation, and appearing concurrent with our work, DebugAgent (Chen et al., 2025) extends HiBug by a search algorithm to identify weak slices. While we also apply attributes to data to perform a subsequent weak slice search, we instead use the less compute intensive, CLIP Radford et al. (2021) model to generate attributes. Additionally, we develop a Bayesian framework to compensate for the label noise that occurs from the attribution.

In contrast to SDMs, local interpretability and feature attribution methods (Ribeiro et al., 2016; Lundberg & Lee, 2017) identify local explanations and not the global systematic weaknesses, while linking the achieved understandability to actionability (Guidotti et al., 2022). In addition, the feature attribution methods themselves are not robust or consistent (Krishna et al., 2022). Similarly, approaches inspired by concept activations like CountTEX (Kim et al., 2023) propose to overcome issues with manual collection of concepts by leveraging CLIP and using text-driven concepts.

### 3 Method

Within this section we explain our proposed modular workflow for weakness detection on the basis of human-understandable semantic dimensions. To this end, we introduce notation regarding metadata and slicing, discuss the generation of metadata, formulate DNN weakness within a Bayesian framework to account for the impact of noise, and lastly detail how such impact can be acknowledged within slice discovery algorithms.

**Notation:** Consider a DNN-under-test (**DuT**)  $M$  trained on some computer vision task. Let  $\mathcal{D}$  be the (test) data containing inputs and corresponding task-related ground-truth. For each sample  $s_i \in \mathcal{D}$ , using some per-sample performance metric (e.g., intersection over union (IoU)) and, if applicable, by applying some threshold, we obtain binarized **DuT** errors defined as  $e_i \in \{0, 1\}$ , i.e., a given sample can be either predicted correctly ( $e_i = 0$ ) or incorrectly ( $e_i = 1$ ) by the **DuT**. Here, we mildly deviate from conventional notation as instead of inputs to the **DuT** we discuss individual samples. While identical for image classification, in

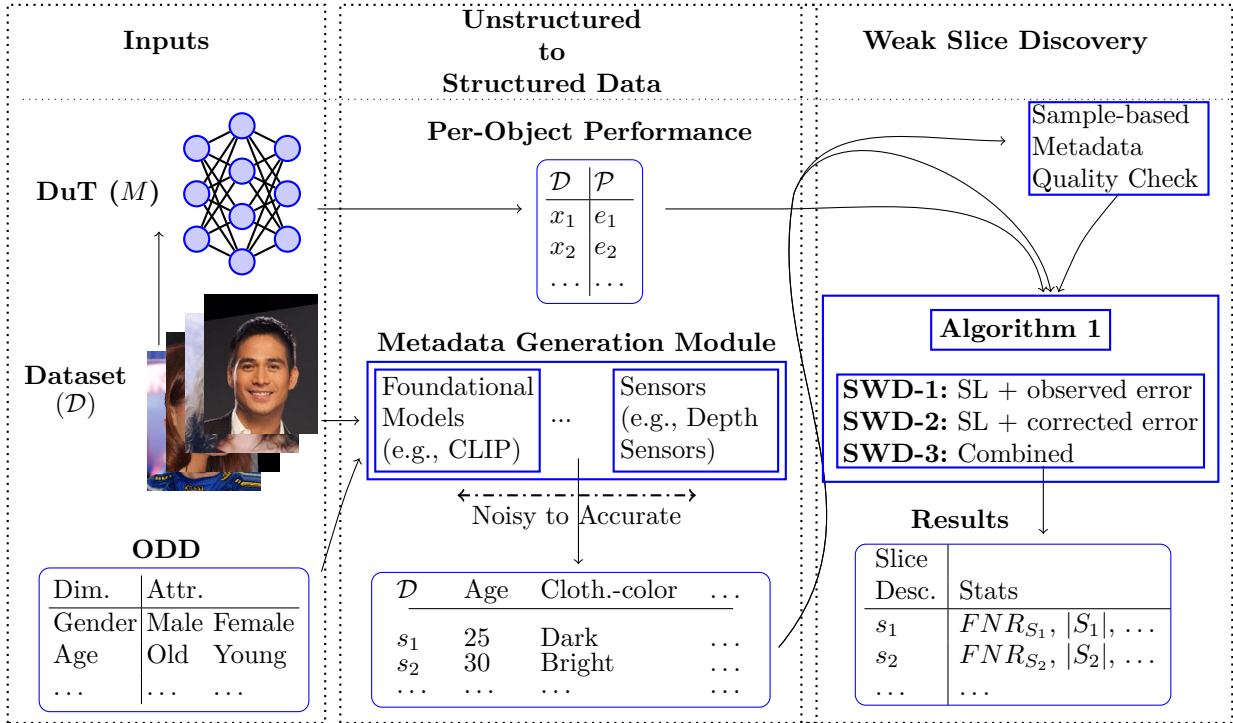


Figure 1: Our proposed modular workflow for finding systematic weaknesses of CV models. Given a model, a test dataset, and an ODD description for the objects we are interested in, our approach builds a database of object-level performance and metadata in a structured format. Weak slice discovery methods are then applied to this database to identify top-k weak slices of the model.

case of object detection, multiple samples (i.e., objects) may be present on a given input image over which inference is performed. Using a set of samples with individual errors  $e_i$  allows us to define slices  $\mathcal{S} \subseteq \mathcal{D}$  of the data and their corresponding (average) error rate  $\bar{e}_{|\mathcal{S}|}$  defined as  $\frac{1}{|\mathcal{S}|} \sum_{s \in \mathcal{S}} e_s$ . It is one of the goals of slice discovery methods to find slices such that  $\bar{e}_{|\mathcal{S}|}$  is significantly worse than the global average  $\bar{e}_{|\mathcal{D}|}$ . However, this constraint alone would be ideally fulfilled by a subset containing all  $s_i$  where  $e_i = 1$ . But, this, in general, would reveal no further information than the known data-points with bad performance.

As motivated in section 1, slice discovery methods aim to provide further information about DNN weaknesses by attempting to find semantically coherent slices. This is typically done by using some scheme that can determine if any specific sample  $s_i$  belongs to the set  $\mathcal{S}$ . The scheme relies on additional information that is not solely provided by the  $e_i$ . This additional information may then be used to infer on the cause of the weakness. Several existing works (d’Eon et al., 2022; Eyuboglu et al., 2022; Jain et al., 2023) base their scheme on distance measures in latent spaces of the samples, such that resulting clusters, i.e., slices, require further interpretation. In contrast, this work bases the information on metadata, more concretely a pre-defined set  $\mathcal{Z}$  of semantic dimensions and corresponding attributes that describe the samples. For instance, in the case of pedestrian detection, such dimensions can be fairness related attributes such as “gender” or “age” with attributes such as “young” or “old” but may also include safety relevant aspects such as “occlusion” or “clothing-color”. Such an approach offers direct interpretability of the slices and selected dimensions can be aligned, e.g., with existing safety considerations in the form of Operational Design Domains (ODDs) of the respective systems. The used set  $\mathcal{Z}$  in this work was inspired by Herrmann et al. (2022) from automotive ODDs.

In fig. 1, our modular workflow is shown, where, using inputs such as, dataset, predefined ODDs, and a DNN-under-test, we transform the task of finding systematic weaknesses in the unstructured data domain into a structured data domain problem. The first module deals with the generation of structured metadata,

see next paragraph, while the second module deals with the slice discovery algorithm that is applied on the generated structured metadata. Having a structured description of the data, we can formulate slices as rules over  $\mathcal{Z}$ , e.g.,  $\text{gender} = \text{male} \wedge \text{occlusion} = (0.9, 1.0]$ . This allows a more probabilistic notation  $p(e|\mathcal{S})$  of the expected error given the slice. Slice discovery is then a task of finding (coherent) conditions  $\mathcal{S}$  such that the conditional expectation is maximized.

**Metadata Generation:** While there is great interest from safety experts and certification bodies in ODDs for safety argumentation, metadata that aligns with the ODD is scarcely available for most, particularly image, domains. Human annotation of such metadata is often out of scope for large datasets due to cost and time constraints. However, an automated metadata generation approach that captures different semantic dimensions of  $\mathcal{Z}$  is feasible with existing technologies. For example, a multi-modal foundational model like CLIP (Radford et al., 2021) with its joint image and text embedding space could be a potential candidate for such automated annotation either out-of-the-box or after fine-tuning. For a given attribute  $a$  we can use CLIP as a zero-shot classification function  $\mathcal{G}$ , which maps a given sample  $s_i$  onto the attributes values, which represent the potential classes. As such, it therefore provides the coherence of the slices discussed above.

Taking the ontology for pedestrians from the automotive domain as a baseline, a qualitative evaluation of CLIP’s capability was done by Gannamaneni et al. (2023). While CLIP achieved SOTA level zero-shot performance for identifying different attributes like gender, skin-color, and age for portrait shots of human faces in the celebA dataset, they observed a drop in performance on real-world datasets containing pedestrians like in the Cityscapes dataset. The drop in performance can be attributed to more challenging conditions such as complex poses, low illumination, high occlusion. This observation, and our experiments below, show that the classification function  $\mathcal{G}$  is subject to varying degrees and types of uncertainty, depending on the dimensions of  $\mathcal{Z}$ : (i) the presence of data based (aleatoric) uncertainties, i.e., where the image resolution is low or the object in question is heavily occluded or distant leading to errors in generated metadata. (ii) the presence of model based (epistemic) uncertainties, i.e., where the function  $\mathcal{G}$  has sub-optimal performance. While (i) can occur in case of both human and CLIP based annotation, (ii) more prominently occurs in non-human, automated labelling.<sup>3</sup> Therefore, any method that aims to consider metadata generated using such techniques should take into account the incurred noisiness in the downstream tasks.

**Bayesian Framework to Account for the Impact of Noise:** To address the uncertain nature of classification, we extend the previous slice notation of the error to the joint? probability  $p(e, \mathcal{C}, \mathcal{S})$ , where  $\mathcal{C}$  represents the outcome of the automated labelling for some attribute of a dimension while  $\mathcal{S}$  denotes the corresponding ground-truth. For simplicity, we drop the indices and make the further assumption that  $\mathcal{S}, \mathcal{C}$  can be seen as binary, i.e. they may either be true ( $\mathcal{S}, \mathcal{C}$ ) or not true ( $\neg\mathcal{S}, \neg\mathcal{C}$ ), respectively. Using Bayes’ Theorem and marginalizing over the  $\mathcal{C}$  or  $\mathcal{S}$  we can express

$$p(e|\mathcal{S}) = p(e|\mathcal{C}, \mathcal{S})r_{\mathcal{C}} + p(e|\neg\mathcal{C}, \mathcal{S})(1 - r_{\mathcal{C}}), \quad (1)$$

$$p(e|\mathcal{C}) = p(e|\mathcal{C}, \mathcal{S})p_{\mathcal{C}} + p(e|\mathcal{C}, \neg\mathcal{S})(1 - p_{\mathcal{C}}). \quad (2)$$

Here,  $p(e|\mathcal{S})$  represents the true slice error while  $p(e|\mathcal{C})$  denotes the observed slice error. Furthermore,  $p_{\mathcal{C}} = p(\mathcal{S}|\mathcal{C})$  and  $r_{\mathcal{C}} = p(\mathcal{C}|\mathcal{S})$  are short-hands for precision and recall of the labelling function  $\mathcal{G}$  as measured towards the ground-truth, and are used in the workflow, fig. 1, for the quality check. A more detailed derivation of the equations can be found in appendix E. Making these relations explicit allows us to investigate the hypothesis typically underlying Slice Discovery Methods in more detail. Namely, purely from an observed subset performance/weakness  $p(e|\mathcal{C})$  one may conclude that a related data property  $\mathcal{S}$  constitutes a weakness of the **DuT** in the sense that also  $p(e|\mathcal{S})$  has a comparable performance/weakness. While in our approach the relation between  $\mathcal{S}$  and  $\mathcal{C}$  is explicit as the latter is given by a classifier for the former, in other approaches d’Eon et al. (2022); Eyuboglu et al. (2022); Jain et al. (2023) the relation is implicit as observed sets  $\mathcal{C}$  are interpreted to indicate a meaning of  $\mathcal{S}$  (typically referred to as slice label). Another assumption typically made is the independence between the labelling function  $\mathcal{G}$  and the **DuT**. Such independence would imply that the errors of the DuT do not depend on the noise introduced by  $\mathcal{G}$ . Specifically, for a semantic attribute, the error rates  $p(e|\mathcal{C}, \mathcal{S})$  when  $\mathcal{G}$  is correct and the error rate  $p(e|\neg\mathcal{C}, \mathcal{S})$  when it is not should be (approximately) equal. However, our experiments indicate that this is not always the case and we therefore

<sup>3</sup>High quality human labelling typically has to take multiple measures to reduce inter-observer variability or epistemic uncertainty in general (e.g. via labelling guides). Within this work, however, we use given human annotation as ground-truth.

denote the difference by

$$\delta p(e|\mathcal{S}) = p(e|\neg\mathcal{C}, \mathcal{S}) - p(e|\mathcal{C}, \mathcal{S}). \quad (3)$$

Please note that  $\delta p$  describes intra-set variances of the error rate in the set  $\mathcal{S}$  and is not a conditional probability on its own. Taking into account this potential dependence, we can derive the true error from the observed error exactly given the performance of the annotation process using

$$p(e|\mathcal{S}) = \underbrace{\frac{p(e|\mathcal{C})p_{-c} + p(e|\neg\mathcal{C})(p_c - 1)}{p_c + p_{-c} - 1}}_{\text{independence assumption}} + \underbrace{\delta p(e|\mathcal{S}) \left( \frac{p_c p_{-c}}{p_c + p_{-c} - 1} - r_c \right) + \delta p(e|\neg\mathcal{S}) \frac{(p_c - 1)p_{-c}}{p_c + p_{-c} - 1}}_{\text{correction terms}}. \quad (4)$$

As long as the independence assumption is (approximately) valid, implying  $\delta p(e|\mathcal{S}) \approx \delta p(e|\neg\mathcal{S}) \approx 0$ , the slice error given the semantic attribute  $\mathcal{S}$  is obtained by separating the two types of observed error probabilities  $p(e|\mathcal{C})$ , which is possible as long as the denominator is non-zero.<sup>4</sup> An analysis of properties of this equation w.r.t. the denominator and the independence of  $\kappa$  terms from  $\delta$  terms allows us to automatically create quality indicators on the validity or invalidity of the obtained corrected slices for attribute  $\mathcal{S}$ . The full derivation and further details regarding quality indicators are in appendix F.

**Weak Slice discovery on Structured ODD data with SliceLine:** We have now established methods to generate metadata and correct for noise during the metadata generation. With this as background, in algorithm 1, we propose a three staged approach for a Systematic Weakness Detector (SWD-1,2,3). In SWD-1, using the generated structured metadata and observed errors  $p(e|\mathcal{C})$ , we can employ algorithms like SliceLine (Sagadeeva & Boehm, 2021) to provide a ranked list of top- $k$  worst performing slices based on a scoring function that takes into account errors and sizes of slices (see eq. (5) in appendix D on how SliceLine works). As we have motivated, the observed errors might not always provide sufficient signal to identify the underlying error (see top row in fig. 2). Therefore, in SWD-2, utilizing eq. (4) to compensate for the noise in the metadata, we provide corrected errors instead of observed errors to SliceLine to provide a second, ranked list of top- $k$  worst performing slices  $\mathcal{S}$ . However, as it requires extensive human effort to identify all parameters in eq. (4), we make a cheaper approximation by only considering the independence assumption part of eq. (4), shown as `computeCorrectedError()` in algorithm 1, and estimate precision values based on human evaluation of metadata quality on  $n = 60$  samples per attribute (see appendix H). These errors are the ones utilized in the scoring function of SliceLine. Based on the slice quality indicators discussed above, we are also able to discard invalid slices due to denominator values close to zero. In addition to SWD-1 and SWD-2, we also consider a merge of the resulting slices from both approaches as this might provide a complementary effect at a cost of loss of precision in identified weak slices as SWD-3. The merge step includes sorting based on slice score from scoring function, removal of duplicate slices, and filtering of invalid slices. The SliceLine hyperparameters therein include the level (maximal search depth), i.e. the maximal number of semantic dimensions considered simultaneously, as well as a cut-off for the necessary slice error  $\bar{e}|_{\mathcal{S}}$  to consider  $\mathcal{S}$  a valid slice.

---

**Algorithm 1:** Systematic Weakness Detector (SWD)

---

**Input:** Metadata  $\{\mathcal{C}_{Z_1}, \mathcal{C}_{Z_2}, \dots\}$ , errors  $e$ , Precision vectors  $\{p_{C_i}\}$ , SliceLine hyper-parameters

**Output:** Top-K slices  $TS$

- 1 **SWD-1: SliceLine with observed errors**  $p(e|\mathcal{C}_i)$ ;
  - 2  $[TS_1] \leftarrow \text{SliceLine}(\{\mathcal{C}_{Z_1}, \mathcal{C}_{Z_2}, \dots\}, e, \text{hyperparameters});$
  - 3 **SWD-2: SliceLine with corrected errors (approximations to  $p(e|\mathcal{S}_i)$ );**
  - 4  $[TS_2, \text{Quality Indicators}] \leftarrow$   
 $\quad \text{SliceLine}(\{\mathcal{C}_{Z_1}, \mathcal{C}_{Z_2}, \dots\}, \text{computeCorrectedError}(e, p_c), \text{hyperparameters});$
  - 5 **SWD-3: Combined Slices;**
  - 6  $[TS] \leftarrow \text{Merge}(TS_1 \cup TS_2);$
  - 7 **return**  $TS$ ;
- 

<sup>4</sup>For the sake of numeric stability, also denominators which are only approximately zero should be discarded.

---

## 4 Proof of Concept with Synthetic Data

To demonstrate the efficacy of our proposed workflow fig. 1, evaluations on synthetic dataset are presented first. This is done to evaluate the impact of noise on the labelling process and the degree to which our approaches can compensate for it. The synthetic data is a tabular dataset containing columns for 9 “real” semantic dimensions for 200 000 samples filled with binary values. To each of the “real” dimensions (GT), a “predicted” metadata column is included, as a proxy for metadata that would be generated by CLIP in our workflow (see fig. 1). Finally, one column contains the binarized **DuT** errors ( $e$ ). The first 4 dimensions are generated to be imbalanced with only 5% of the samples belonging to attribute “1”. The other 5 dimensions are generated such that both attributes have equal distribution. The error column is chosen such that weak slices are induced for the ground truth attributes.

We consider three regimes of noise, i.e., different quality of labelling of the simulated annotation process: (i) a regime of “good” quality CLIP labelling, represented with  $p_C$  being above 80%, (ii) a regime of “medium” quality CLIP labelling, represented with  $p_C$  between 40% to 70%, and (iii) a regime of “bad” quality CLIP labelling, represented with  $p_C$  being above 10% to 40%. For all three regimes, we consider 100 runs of the experiments to account for statistical influence. Further details about the dataset generation can be found in appendix B. In fig. 2, on the top row, the error distributions show how labelling quality impacts the spread of error between attributes for each semantic dimension, that is the upper and lower ends of the bars are given by the error rates for  $\bar{e}|_{\mathcal{S}}$ ,  $\bar{e}|_{-\mathcal{S}}$  and similarly using  $\mathcal{C}$  or the corrected errors. In the good labelling quality regime, as expected, observed errors and corrected errors both display the same spread as the GT error. But when labelling quality is medium or bad (where impact of eq. (4) is stronger), spread of observed error is significantly lower than that of corrected error. In contrast, corrected error overestimates what true error (GT) would be. From a safety perspective, we believe it is better to overestimate the systematic error within a DNN than to underestimate it which the corrected approach does. In the bottom row, we evaluate the results of SWD-1,2,3. This is shown by comparing how well the three approaches recover the top- $k$  weak slices by comparison against  $k$  slices from Oracle, i.e., situation where we have access to perfect “GT” labelling quality annotation. Precision and recall are calculated for the three data quality regimes w.r.t. the ideal case by considering the overlap of slices at increasing levels of  $k$ . Note that precision and recall in this figure refer to quality metrics on weak slice discovery and not precision and recall of the CLIP labelling. While, at level 2, the maximum number of slices  $k$  is 162 for 9 binarized dimensions<sup>5</sup>, we consider only slices fulfilling the cut-off requirement as a weak slice. Of those 162 slices, only  $\sim 30$  are identified as weak slices. While under good labelling quality, slices identified by the three approaches basically have 100% overlap with the Oracle, under medium and strong label noise, SWD-3 shows significantly more recall than SWD-1 and marginally over SWD-2. This, however, comes with a small loss in precision. In cases of strong noise, SWD-1 only recovers a few slices where error signal is dominant which explains the high precision at the cost of low recall. SWD-3, on the other hand, has a reduced precision but recovers most of the weak slices identified by Oracle. For the rest of the paper, we primarily focus on slices identified by SWD-3.

## 5 Evaluations of real-world DNNs

In this section, we first present our experimental setup. We then show the evaluation of our systematic weaknesses detection method on a publicly available pre-trained model for the CelebA dataset. Here, the dataset’s rich meta-data annotation allows us to investigate the influence of noisy metadata annotation. In addition, we compare against SOTA SDM methods to evaluate our claim that adherence to ODD descriptions is useful to end users (e.g., safety experts, ML developers). Subsequently, we present the insights gained by using our approach on DNNs trained on autonomous driving datasets.

---

<sup>5</sup> $9 \times 2 + \binom{9}{2} \times 2^2$

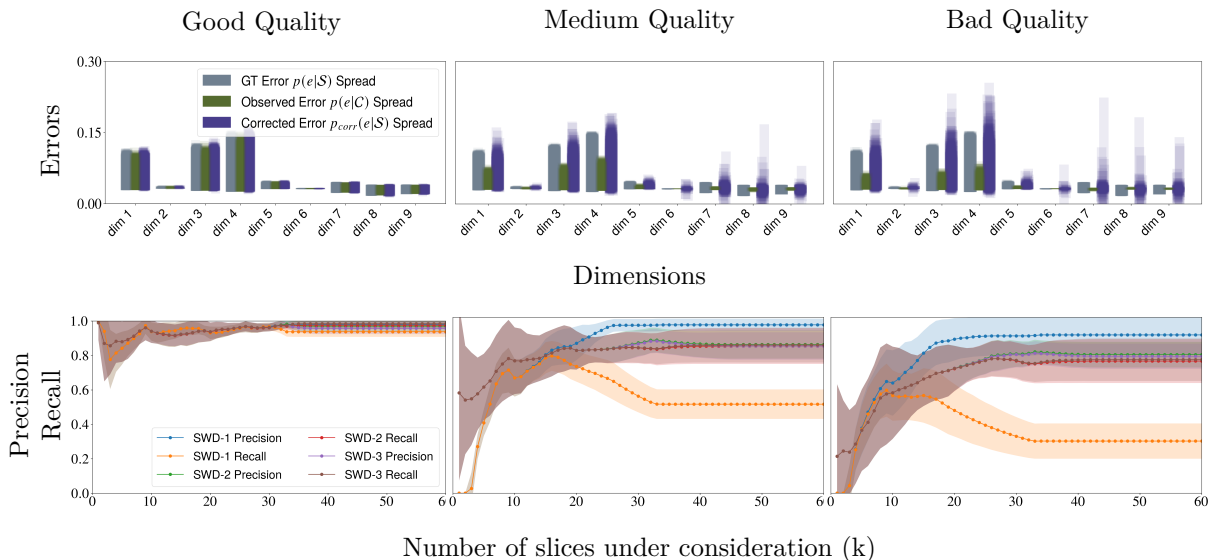


Figure 2: Based on labelling quality, we divide the generated datasets into (i) good quality (left), (ii) medium quality (middle), and (iii) bad quality (right). In three cases, we look at the spread of error in GT ( $p(e|\mathcal{S})$ ), Observed ( $p(e|\mathcal{C})$ ), and Corrected ( $p(e|\mathcal{S})$ ). In the second row, corresponding performance in terms of precision and recall of SWD-1,2,3 are shown. Precision and Recall in this figure are metrics to evaluate weak slice recovery and are not related to labelling quality. The legend for both rows are presented on the figures on left.

## 5.1 Experimental Setup

**Datasets and Models:** Four pre-trained models, ViT-B-16 (Dosovitskiy et al., 2020)<sup>6</sup>, Faster R-CNN (Ren et al., 2015)<sup>7</sup>, SETR PUP (Zheng et al., 2021)<sup>8</sup>, PanopticFCN (Li et al., 2021) are evaluated using four public datasets (CelebA (Liu et al., 2015), BDD100k (Yu et al., 2020), Cityscapes (Cordts et al., 2016), and RailSem19 (Zendel et al., 2019)), respectively. We restrict the number of combinations (level) to 2 in this work. However, as discussed in appendix H, our approach allows for correction of errors even at higher levels of combinations. We utilize the cut-off for slice error as  $1.5 * \bar{e}_{|\mathcal{S}}$  for all experiments except evaluation of PanopticFCN. Here, we utilize the cut-off for slice error as  $1.0 * \bar{e}_{|\mathcal{S}}$  as the global **DuT** error is quite high. For the detailed experimental setup, please refer to appendix A. To foster reproducibility, code and the prompts used for metadata generation with CLIP will be provided.

## 5.2 Evaluation of our Systematic Weaknesses Detection Method

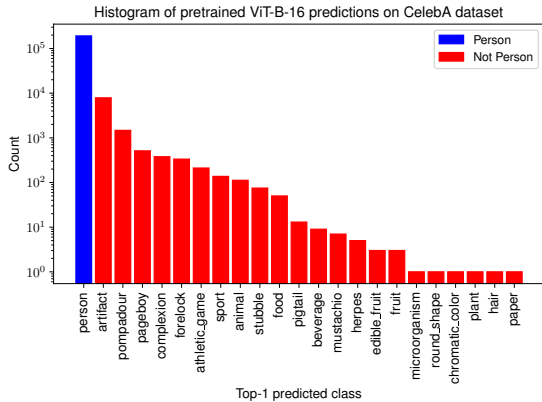
**Evaluating a ViT Model on CelebA:** As our first experiment, we evaluate the weaknesses of the ViT-B-16 (Dosovitskiy et al., 2020) model (**DuT**) trained on ImageNet21k (Ridnik et al., 2021). We use the model for the targeted task of identifying the class “person” in the CelebA dataset (Liu et al., 2015) as a real-world proof of concept for our approach. Due to the extensive range of label categories in ImageNet (Deng et al., 2009) and the significant noise in labelling style, models trained on the full ImageNet dataset or its standard subset ImageNet1k (Russakovsky et al., 2015) can suffer from systematic weaknesses. For example, although the primary foreground object in an image might be a human, in some instances, the image can be labelled as belonging to the class “person” while in other, similar instances, the label might be about more granular classes like “bride” or “guitarist”. To fix this issue, (Ridnik et al., 2021) proposed 11 hierarchies based on WordNet (Miller, 1995) semantic trees such that classes at higher hierarchy levels are superclasses that subsume classes at lower hierarchy levels. However, despite these efforts, considerable label noise in terms of

<sup>6</sup><https://github.com/huggingface/pytorch-image-models>

<sup>7</sup><https://github.com/SysCV/bdd100k-models/tree/main/det>

<sup>8</sup><https://github.com/open-mmlab/mmdetection>





| Slice Description                 | Slice $\mathcal{S}_1$ | Slice Statistics  |
|-----------------------------------|-----------------------|---|
| wearing-hat: true<br>beard: false |                       | Slice Size $ \mathcal{S} $ : 7600<br>$FNR$ of Slice: 0.6856<br>Performance degradation: -0.6304 |



Figure 3: Left: The hierarchy level-0 (Ridnik et al., 2021) predictions of the pre-trained ViT-B-16 model on the full CelebA dataset converted into a binary classification problem. While a majority of the predictions are correct, there is a non-trivial subset of images with systematic errors due to label overlap issues. Right: Top-1 weak slice, identified by SWD-3, of a ViT-B-16 classification model trained on ImageNet21k and evaluated on the full celebA dataset. The statistics provide a quantitative evaluation of the entire slice. For qualitative evaluation, we provide some sample images from the slice.

class overlap still persists. For instance, humans holding specific objects might occur on the same hierarchy level as the class “artifact” or “person”. Similar issues exist, e.g., for hairstyles (see “pompadour” existing on the same level as “person”). For a further analysis also see the work of (Northcutt et al., 2021).

Earlier works (Beyer et al., 2020; Shankar et al., 2020) have proposed using multi-label evaluation metrics as a way to deal with label noise. However, we consider the simplified task of identifying a dedicated class, “Person”, in a dataset with only human faces (celebA) by focusing on the top-1 class predictions for level-0 of the label hierarchy proposed in ImageNet21k. We obtain an accuracy of 94.44% on the 202 599 images in the CelebA dataset. The softmax of the top-1 prediction, see fig. 3, shows, besides the “person” class the presence of several other classes, most prominently “artifact” and “pompadour”. As this model is commonly used as a pre-trained backbone for various applications, uncovering potential shortcomings might also be beneficial for potential downstream use cases of various types. Furthermore, the CelebA dataset serves as an ideal testing ground for approaches identifying systematic weaknesses due to the availability of the ground-truth metadata attributes. As an ODD for this test case, we propose a simplified subset of these available metadata attributes in analogy to the work of (Gannamaneni et al., 2023), for details see appendix C. As proposed in our workflow, we generate metadata using CLIP for the given ODD dimensions. Subsequently, the generated metadata is combined with the softmax values of the class “person”.

**Weak Slice Discovery** As CelebA dataset contains annotated metadata for 40 attributes, we have access to noiseless metadata which when used with SliceLine can be considered as “Oracle” approach. In table 1, we present the top-5 slices identified by SWD-3 and compare this against SWD-1 and Oracle to highlight the importance of error correction. From the slice descriptions, all the identified weak slices contain some variation of the semantic concept “wearing hat”. The discovery of this slice can be seen within the context of the frequent misclassification of images as class “artifact” by the **DuT**. In these cases, the model likely focuses on the hats as the foreground object and predicts the class “artifact”. To evaluate the quality of the identified slices, we define  $FNR|_{\mathcal{S}}$  as the false negative rate obtained on the slice  $\mathcal{S}$ . From the column displaying ranking of slices by each method, we observe that both SWD-1 and SWD-3 identify 3 out of top-5 slices of Oracle. However, whereas the  $FNR$  of SWD-1 underestimates the  $FNR$  of Oracle, SWD-3 effectively corrects the errors. For instance, the difference between the  $FNR$  of Oracle and SWD-1 is 0.3, whereas for SWD-3, it is only 0.07. A thorough evaluation of our approach on top-60 slices shown in fig. 5

---

in appendix I reveal that SWD-3 obtains 100% recall of weak slices at the cost of reduction in precision. From a safety perspective, given noisy labelling, this is preferable over not detecting weak slices.

**Comparison to SOTA SDM method** In addition to evaluation of SWD-3, we compare three SOTA methods DOMINO (Eyuboglu et al., 2022), Spotlight (d’Eon et al., 2022), and SVM FD Jain et al. (2023) against the Oracle. Similar to our work, DOMINO and SVM FD use CLIP (ViT L/14) in their workflow. However, they encode the images in the CLIP embedding space and then search for weak slices without explicitly enforcing any semantic concepts. To describe the slices, both approaches perform an additional step, where the identified slices are explained using text from large language models. In contrast, Spotlight directly uses the embedding space of the **DuT** to cluster weak slices and provides no descriptions of the identified slices. The former methods follow a broader trend (like us) of using foundational models like CLIP in testing smaller models. However, they do not thoroughly address limitations in CLIP’s capabilities and the limitations of their approaches w.r.t. actionability when the slice descriptions are not very meaningful. Our approach tackles both these limitations as we address noise in CLIP labelling and also correctness of descriptions. However, our approach is limited to identifying weaknesses w.r.t. dimensions in  $\mathcal{Z}$  while the other methods do not have this limitation and therefore could identify novel weaknesses. This advantage of SOTA methods, however, as will be shown below, can only be realised if the description or coherence of slices is understandable and actionable to the end-user. To assess actionability of the SOTA methods, we consider (i) slice descriptions based on the methods themselves, (ii) slice coherence based human inspection, and (iii) slice coherence based on overlap with top-5 slices of Oracle.

The qualitative results and slice descriptions are provided in appendix J. We identified that DOMINO descriptions can be very generic and not helpful for identifying the unique attributes of a slice. This problem was also discussed in other works (Jain et al., 2023; Gao et al., 2023). For Spotlight, descriptions are not available as part of the method. In contrast, in SVM FD, the slice description is targeted and covers one dimension of the weak slice identified by Oracle, namely, “wearing hat”. However, as shown earlier, the weaknesses identified from Oracle stem from combination of semantics. Therefore, slice descriptions from the SOTA methods are not enough for actionability. Second, to evaluate the coherence of the slices further, we manually inspect a sample of the images from a slice to identify the semantics. Such an approach is necessary for all methods that do not provide slice descriptions. For such manual inspection to identify slice coherence, we consider samples from the slice and samples from the remaining data (last column) as a form of control group. For top-1 slices of all three approach, it is hard to determine what uniquely constitutes the top-1 slice when considering combination of semantics. Furthermore, such an exercise is time intensive and might potentially uncover spurious patterns.

Finally, to evaluate slice coherence based on overlap with slices from Oracle, we present in table 2 the top-1 slice identified by each method, their corresponding statistics and the overlap (Jaccard Similarity Coefficient) of the top-1 slice with top-5 slices of Oracle. From the slice statistics, it can be observed that the methods recover slices with significant performance degradation and  $FNR$ . Here, we define performance degradation as  $FNR|_{\mathcal{D}} - FNR|_{\mathcal{S}}$ . However, the overlap of the top-1 slices with top-5 of Oracle is quite low. This indicates that the methods might be uncovering weaknesses w.r.t. dimensions not present in the ODD. However, with no useful descriptions, the actionability of these approaches is low. Furthermore, we evaluate the overlap of top-1 slice with a slice that is purely made up of FNs of the **DuT**. High values on this column might indicate that priority is given to identifying FNs rather than semantic coherence as it is unlikely that all weaknesses of a DNN can be explained by one semantic concept. Therefore, grouping all FNs into one slice would be counterproductive. As DOMINO captures 64% of all false negatives into its top-1 slice, it is unlikely that such a slice is actionable. In contrast, Spotlight and SVM FD capture fewer FNs in top-1 slice. Therefore, they might be capturing some form of combination of semantics. Based on these evaluations, we conclude that SOTA methods, when integrated with improved slice description techniques, could complement our approach. However, in its current form, our approach offers greater actionability due to its inherent slice descriptions.

### 5.3 Insights on SOTA Pedestrian Detection Models

Having shown the benefits of our proposed method, we evaluate a more safety-relevant task of pedestrian detection using models trained on real-world autonomous driving (AD) datasets to identify their system-

| Slice           | Slice Description                                    | SWD-3       |                   |              | SWD-1       |                   |       | Oracle      |                   |       |
|-----------------|--|-------------|-------------------|--------------|-------------|-------------------|-------|-------------|-------------------|-------|
|                 |  | rank( $S$ ) | $ \mathcal{S}_1 $ | $FNR_{corr}$ | rank( $S$ ) | $ \mathcal{S}_1 $ | $FNR$ | rank( $S$ ) | $ \mathcal{S}_1 $ | $FNR$ |
| $\mathcal{S}_1$ | <b>Wearing-Hat:</b> True<br><b>Beard:</b> False      | 1           | 7600              | 0.69         | 6           | 12152             | 0.33  | 2           | 6267              | 0.51  |
| $\mathcal{S}_2$ | <b>Wearing-Hat:</b> True<br><b>Smiling:</b> False    | 2           | 5132              | 0.60         | 3           | 8573              | 0.36  | 9           | 6476              | 0.35  |
| $\mathcal{S}_3$ | <b>Wearing-Hat:</b> True<br><b>Gender:</b> Female    | 3           | 4435              | 0.61         | 2           | 7393              | 0.38  | 1           | 2947              | 0.68  |
| $\mathcal{S}_4$ | <b>Wearing-Hat:</b> True<br><b>Age:</b> Young        | 4           | 7974              | 0.54         | 4           | 12758             | 0.34  | 3           | 6937              | 0.50  |
| $\mathcal{S}_5$ | <b>Wearing-Hat:</b> True<br><b>Eyeglasses:</b> False | 5           | 8606              | 0.54         | 5           | 12594             | 0.33  | 6           | 8417              | 0.45  |

Table 1: Evaluation of top-5 slices of SWD-3 (see algorithm 1) by comparing its statistics with corresponding slice statistics of SWD-1 and Oracle. The rank column indicates the slice ranking in each approach. Both SWD-1 and SWD-3 recover 3 out of 5 weak slices in top-5 of Oracle weak slices.

| Method    | Slice Statistics     |                   |                        | Slice Coherence with Attributes            |                                     |                                     |                                     |                                     | Overlap with FN $\ddagger$   |
|-----------|----------------------|-------------------|------------------------|--|-------------------------------------|-------------------------------------|-------------------------------------|-------------------------------------|--|
|           | Perf. degr.          | Size              |                        | Overlap with Oracle top-5 slices $\dagger$ |                                     |                                     |                                     |                                     |  |
|           | $FNR _{\mathcal{D}}$ | $ \mathcal{S}_1 $ | $FNR _{\mathcal{S}_1}$ | $J(\mathcal{S}_1, \mathcal{S}_1^O)$        | $J(\mathcal{S}_1, \mathcal{S}_2^O)$ | $J(\mathcal{S}_1, \mathcal{S}_3^O)$ | $J(\mathcal{S}_1, \mathcal{S}_4^O)$ | $J(\mathcal{S}_1, \mathcal{S}_5^O)$ | $\frac{ \mathcal{S}_1 \cap \mathcal{S}_{FN} }{ \mathcal{S}_{FN} }$ |
| DOMINO    | -0.5629              | 11726             | 0.6181                 | 0.13                                       | 0.19                                | 0.20                                | 0.21                                | 0.24                                | 0.64   |
| Spotlight | -0.8622              | 4050              | 0.9179                 | 0.32                                       | 0.32                                | 0.32                                | 0.31                                | 0.31                                | 0.33   |
| SVM FD    | -0.3844              | 2642              | 0.4295                 | 0.11                                       | 0.15                                | 0.16                                | 0.16                                | 0.16                                | 0.24   |

Table 2: Comparison of three metadata-free SOTA methods with top-5 slices of Oracle.  $J(\mathcal{S}_1, \mathcal{S}_x^O)$  indicates the Jaccard similarity coefficient between the two slices. appendix J contains samples from each slice of the SOTA methods along with slice descriptions and statistics.  $\dagger$  - Higher values are better,  $\ddagger$  - Low values indicate that slice does not contain “significant” weaknesses. Higher values indicate that potentially all weaknesses of **DuT** are in one slice.

atic weaknesses when predicting the class “pedestrian”. For this, we require pedestrian level performances (intersection-over-union (IoU)) and metadata. To avoid noisy labelling in our metadata generation step, we perform some additional steps which were not required for the previous experiment. First, we crop all the pedestrians from the images and consider these crops as  $\mathcal{D}$ . This is done to focus the CLIP model only on the pedestrians during metadata generation.<sup>9</sup>

Second, we calculate the pixel area of the pedestrians based on the ground-truth bounding box area and use this to filter  $\mathcal{D}$  by removing pedestrians that occupy small pixel areas (“smaller” pedestrians). Such filtering is necessary as: (i) Due to low resolution and high pixelation of “smaller” sized pedestrians, i.e., there is high aleatoric uncertainty regarding the correct labels affecting both CLIP and human labellers in understanding the image content (e.g., to determine gender, age, etc.). (ii) “Smaller” pedestrians are more likely to be farther from the ego-vehicle<sup>10</sup> and, therefore, might be considered less safety-relevant (in terms of vehicle breaking time). (iii) As small size can be strongly correlated to performance (due to distance (Gannamaneni et al.,

<sup>9</sup>To avoid that the aspect ratio of pedestrians is changed by the CLIP pre-processing, we use padding to obtain square crops.

<sup>10</sup>Unless if small size is due to occlusion. For BDD100k dataset, where occlusion is available as annotation, we show impact of occlusion as well

2021) or occlusion), such signal can strongly dominate the search for systematic weaknesses by SliceLine, thereby not providing any novel insights in terms of systematic weaknesses. For this reason, we remove the low-resolution “smaller” pedestrians to improve the quality of the metadata generation and gain further novel insights about model failures w.r.t. more safety-relevant pedestrians.

The metadata generation using CLIP is performed using ODDs more suitable for automotive context (see appendix C). We also perform a manual evaluation of a subset of images ( $n = 60$ ) for each attribute in each dataset to evaluate the quality of the generated metadata by estimating the precision  $p_C$  and recall  $r_C$  (as discussed in section 3) and show the results in table 3.

| Sem. dim.       | Attri.       | Estimated Precision $p_C$ |                 |                 | Estimated Recall $r_C$ |                 |                 |
|-----------------|--------------|---------------------------|-----------------|-----------------|------------------------|-----------------|-----------------|
|                 |              | BDD100k                   | Cityscapes      | RailSem19       | BDD100k                | Cityscapes      | RailSem19       |
| Age             | Adult        | $0.95 \pm 0.03$           | $0.99 \pm 0.02$ | $0.97 \pm 0.02$ | $0.76 \pm 0.03$        | $0.70 \pm 0.02$ | $0.55 \pm 0.02$ |
|                 | Young        | $0.69 \pm 0.06$           | $0.56 \pm 0.06$ | $0.42 \pm 0.06$ | $0.93 \pm 0.06$        | $0.97 \pm 0.06$ | $0.94 \pm 0.06$ |
| Gender          | Female       | $0.84 \pm 0.05$           | $0.97 \pm 0.02$ | $0.85 \pm 0.04$ | $0.90 \pm 0.05$        | $0.95 \pm 0.02$ | $0.87 \pm 0.04$ |
|                 | Male         | $0.94 \pm 0.03$           | $0.97 \pm 0.02$ | $0.94 \pm 0.03$ | $0.88 \pm 0.03$        | $0.97 \pm 0.02$ | $0.92 \pm 0.03$ |
| Cloth.-color    | Bright-color | $0.81 \pm 0.05$           | $0.85 \pm 0.04$ | $0.79 \pm 0.05$ | $0.30 \pm 0.05$        | $0.23 \pm 0.04$ | $0.66 \pm 0.05$ |
|                 | Dark-color   | $0.76 \pm 0.05$           | $0.65 \pm 0.06$ | $0.82 \pm 0.05$ | $0.96 \pm 0.05$        | $0.97 \pm 0.06$ | $0.89 \pm 0.05$ |
| Skin-color      | Dark         | $0.82 \pm 0.05$           | $0.55 \pm 0.06$ | $0.56 \pm 0.06$ | $0.92 \pm 0.05$        | $0.71 \pm 0.06$ | $0.76 \pm 0.06$ |
|                 | White        | $0.99 \pm 0.02$           | $0.95 \pm 0.03$ | $0.89 \pm 0.04$ | $0.96 \pm 0.02$        | $0.91 \pm 0.03$ | $0.75 \pm 0.04$ |
| Blurry          | True         | $0.71 \pm 0.06$           | $0.63 \pm 0.06$ | $0.87 \pm 0.04$ | $0.42 \pm 0.06$        | $0.87 \pm 0.06$ | $0.64 \pm 0.04$ |
|                 | False        | $0.48 \pm 0.06$           | $0.95 \pm 0.03$ | $0.84 \pm 0.05$ | $0.74 \pm 0.06$        | $0.82 \pm 0.03$ | $0.95 \pm 0.05$ |
| Constru.-Worker | False        | -                         | -               | $0.97 \pm 0.02$ | -                      | -               | $0.98 \pm 0.02$ |
|                 | True         | -                         | -               | $0.65 \pm 0.06$ | -                      | -               | $0.55 \pm 0.06$ |

Table 3: The estimated precision and recall using our proposed approach for evaluating the quality of the generated metadata. Here, we provide the mean and  $\sigma/2$ , for  $n$  of 60, of the estimated precision and recall. Certain dimensions like occlusion are available as part of the datasets themselves. We do not perform human-evaluation for these dimensions but these are considered in the weak-slice search.

In this evaluations, using SWD-3, we evaluate the weaknesses of an object detection model (Faster R-CNN), a segmentation model (SeTR PUP), and a panoptic segmentation model (Panoptic-FCN). The models are evaluated on their respective datasets, i.e., BDD100k, Cityscapes, and RailSem19. Samples of image crops of the identified top-1 weak slice for each experiment are shown in fig. 4 (see figs. 10 to 12 in appendix J for top-5 weak slices). In table 4, we present the largest and the worst performing slice from the top-5 to provide insights about the three models. In all three experiments, the performance degradation of the identified slices is significant. “Occlusion”, “dark” skin-color and clothing-color are reoccurring slice descriptions for the first two models, which are tested on datasets that contain images with many nighttime scenes (BDD100k) or relatively high gray-toned scenes (Cityscapes). In contrast, the third model, which contains relatively brighter scenes, has a significant weakness for the dimension “age”. The estimated precision  $p_C$  and recall  $r_C$  in table 3 were provided as input to algorithm 1 to obtain these slices and ascertain the quality of the identified weaknesses. Therefore, in contrast to SOTA SDMs, our approach identifies human-understandable safety-relevant systematic weaknesses in DNNs used for real-world applications.

## 6 Conclusion

In this work, we present a modular workflow for our Systematic Weakness Detector (SWD) to analyse the systematic weaknesses of DNNs that perform classification, object detection, and semantic segmentation tasks on image data. In the first step, we overcome the problem of missing metadata by generating metadata with a foundation model. Subsequently, in the second step, we perform slice discovery on the structured metadata, which comprises of DNN-under-test’s per-object performance and previously acquired per-object metadata. Using our workflow, we transform the slice discovery of unstructured image data into an (approximate) slice



Figure 4: Left: Samples from top-1 weak slice of a Faster R-CNN object detector trained and evaluated on BDD100k dataset. Middle: Samples from top-1 weak slice of SeTR model trained and evaluated on Cityscapes dataset. Right: Samples from top-1 weak slice of a Panoptic-FCN model trained and evaluated on RailSem19 dataset.

discovery problem on structured data. In addition, we study the impact of noisy labelling in a Bayesian framework and operationalize it by integrating error correction and slice validity based on quality indicators into our approach. In the ablation experiments, we show that our SWD detects the same weak slices as would be identified in hypothetical cases where we have access to perfect metadata. The primary advantage of our method, in comparison to SOTA approaches, is that the identified weak slices are aligned with human-understandable semantic concepts that can be derived from a description of the ODD. As upcoming safety and trustworthy AI specifications require evidences for building safety argumentations w.r.t. such ODDs, the results from our approach can directly contribute. In addition, the identification of human-understandable weak slices enables ML developers to take mitigation actions, such as a targeted acquisition or generation of data, addressing the weaker slices, and, thus, facilitating effective re-training with a limited acquisition budget. Furthermore, we show that our approach has clear advantages over several metadata-free SOTA methods by giving more actionable results and we demonstrate the applicability of our approach by identifying systematic weaknesses in multiple AD datasets. For this, we also provide a quantitative evaluation of the quality of the generated metadata.

Our workflow does have certain limitations. Primarily, a minimum metadata labelling quality is required for the discovered slices to be meaningful. In addition to our proposed metadata quality estimation, future works could, therefore, focus on improving metadata quality by human correction of a subset of the generated metadata, fine-tuning (Eyuboglu et al., 2022) of CLIP, metadata acquisition from other sources (e.g., depth sensor). Secondly, all approaches based on ODD definitions, like ours or PromptAttack (Metzen et al., 2023), would suffer from a lack of completeness of the semantic concepts in the ODD. A potential solution could be in the direction of Gannamaneni et al. (2024) by performing a root-cause analysis of found weaknesses.

| Model & Dataset           | Largest Slice (in top-5)      |          |             | Worst Performing Slice (in top-5) |          |             |
|---------------------------|-------------------------------|----------|-------------|-----------------------------------|----------|-------------|
|                           | $\frac{ S }{ \mathcal{D} }\%$ | $FNR _S$ | Perf. Degr. | $\frac{ S }{ \mathcal{D} }\%$     | $FNR _S$ | Perf. Degr. |
| Faster R-CNN<br>BDD100k   | 34.44%                        | 0.1263   | -0.0693     | 14.22%                            | 0.2206   | -0.1636     |
| SeTR<br>Cityscapes        | 13.34%                        | 0.0594   | -0.0446     | 9.24%                             | 0.1046   | -0.0897     |
| Panoptic-FCN<br>RailSem19 | 25.49%                        | 0.8663   | -0.222      | 8.13%                             | 1.0      | -0.4602     |

Table 4: Quantitative analysis of three pre-trained autonomous driving models (results are only for SWD-3). From the top-5 weak slices, we show the largest slice and the weakest performing slice. Please refer to the appendix J for the top-5 slices.

---

Such approaches could address potential issues between correlation and causation for found small slices. In addition, SDMs based on test dataset evaluation can suffer from insufficient coverage of the application domain by the test dataset. Both aspects become more relevant with the increasing broadness of the assumed ODD scope. For instance, if one intends to investigate false positives in object detection, the description would, effectively, contain most other objects (and parts thereof) that could appear in the scene.

While we, therefore, limit our scope to the more narrowly defined false negatives, our approach still provides valuable insights into, often more critical, missed detections in terms of human-understandable and, thereby, actionable weak slices. We believe that such results can contribute to the development of trustworthy AI models and their safety.

## References

- Martin Atzmueller. Subgroup discovery. *Wiley Interdisciplinary Reviews: Data Mining and Knowledge Discovery*, 5(1):35–49, 2015.
- Lucas Beyer, Olivier J Hénaff, Alexander Kolesnikov, Xiaohua Zhai, and Aäron van den Oord. Are we done with imagenet? *arXiv preprint arXiv:2006.07159*, 2020.
- Joy Buolamwini and Timnit Gebru. Gender shades: Intersectional accuracy disparities in commercial gender classification. In *Conference on fairness, accountability and transparency*, pp. 77–91. PMLR, 2018.
- Simon Burton, Christian Hellert, Fabian Hüger, Michael Mock, and Andreas Rohatschek. *Safety Assurance of Machine Learning for Perception Functions*, pp. 335–358. Springer International Publishing, Cham, 2022. doi: 10.1007/978-3-031-01233-4\_12. URL [https://doi.org/10.1007/978-3-031-01233-4\\_12](https://doi.org/10.1007/978-3-031-01233-4_12).
- Muxi Chen, YU LI, and Qiang Xu. Hibus: On human-interpretable model debug. In A. Oh, T. Naumann, A. Globerson, K. Saenko, M. Hardt, and S. Levine (eds.), *Advances in Neural Information Processing Systems*, volume 36, pp. 4753–4766. Curran Associates, Inc., 2023. URL [https://proceedings.neurips.cc/paper\\_files/paper/2023/file/0f53ecc0d36a5d5d3d3e94d42c4b23ca-Paper-Conference.pdf](https://proceedings.neurips.cc/paper_files/paper/2023/file/0f53ecc0d36a5d5d3d3e94d42c4b23ca-Paper-Conference.pdf).
- Muxi Chen, Chenchen Zhao, and Qiang Xu. Debugagent: Efficient and interpretable error slice discovery for comprehensive model debugging. *arXiv preprint arXiv:2501.16751*, 2025.
- Yeounoh Chung, Tim Kraska, Neoklis Polyzotis, Ki Hyun Tae, and Steven Euijong Whang. Slice finder: Automated data slicing for model validation. In *2019 IEEE 35th International Conference on Data Engineering (ICDE)*, pp. 1550–1553. IEEE, 2019.
- Marius Cordts, Mohamed Omran, Sebastian Ramos, Timo Rehfeld, Markus Enzweiler, Rodrigo Benenson, Uwe Franke, Stefan Roth, and Bernt Schiele. The cityscapes dataset for semantic urban scene understanding. In *Proceedings of the IEEE/CVF Conference on Computer Vision and Pattern Recognition*, pp. 3213–3223, 2016.
- Jia Deng, Wei Dong, Richard Socher, Li-Jia Li, Kai Li, and Li Fei-Fei. Imagenet: A large-scale hierarchical image database. In *2009 IEEE conference on computer vision and pattern recognition*, pp. 248–255. Ieee, 2009.
- Greg d’Eon, Jason d’Eon, James R Wright, and Kevin Leyton-Brown. The spotlight: A general method for discovering systematic errors in deep learning models. In *2022 ACM Conference on Fairness, Accountability, and Transparency*, pp. 1962–1981, 2022.
- Alexey Dosovitskiy, Lucas Beyer, Alexander Kolesnikov, Dirk Weissenborn, Xiaohua Zhai, Thomas Unterthiner, Mostafa Dehghani, Matthias Minderer, Georg Heigold, Sylvain Gelly, et al. An image is worth 16x16 words: Transformers for image recognition at scale. *arXiv preprint arXiv:2010.11929*, 2020.
- EASA. Easa concept paper: guidance for level 1 & 2 machine learning applications. proposed issue 02. Technical report, EASA, 02 2023.

- 
- Sabri Eyuboglu, Maya Varma, Khaled Saab, Jean-Benoit Delbrouck, Christopher Lee-Messer, Jared Dunmon, James Zou, and Christopher Ré. Domino: Discovering systematic errors with cross-modal embeddings. *arXiv preprint arXiv:2203.14960*, 2022.
- Sujan Gannamaneni, Sebastian Houben, and Maram Akila. Semantic concept testing in autonomous driving by extraction of object-level annotations from carla. In *Proceedings of the IEEE/CVF International Conference on Computer Vision (ICCV) Workshops*, pp. 1006–1014, October 2021.
- Sujan Sai Gannamaneni, Arwin Sadaghiani, Rohil Prakash Rao, Michael Mock, and Maram Akila. Investigating clip performance for meta-data generation in ad datasets. In *Proceedings of the IEEE/CVF Conference on Computer Vision and Pattern Recognition (CVPR) Workshops*, pp. 3840–3850, June 2023.
- Sujan Sai Gannamaneni, Michael Mock, and Maram Akila. Assessing systematic weaknesses of dnns using counterfactuals. *AI and Ethics*, pp. 1–9, 2024.
- Irena Gao, Gabriel Ilharco, Scott Lundberg, and Marco Tulio Ribeiro. Adaptive testing of computer vision models. In *Proceedings of the IEEE/CVF International Conference on Computer Vision*, pp. 4003–4014, 2023.
- Robert Geirhos, Jörn-Henrik Jacobsen, Claudio Michaelis, Richard Zemel, Wieland Brendel, Matthias Bethge, and Felix A Wichmann. Shortcut learning in deep neural networks. *Nature Machine Intelligence*, 2(11):665–673, 2020.
- Riccardo Guidotti, Anna Monreale, Salvatore Ruggieri, Francesca Naretto, Franco Turini, Dino Pedreschi, and Fosca Giannotti. Stable and actionable explanations of black-box models through factual and counterfactual rules. *Data Mining and Knowledge Discovery*, pp. 1–38, 2022. doi: <https://doi.org/10.1007/s10618-022-00878-5>.
- Martin Herrmann, Christian Witt, Laureen Lake, Stefani Guneshka, Christian Heinzemann, Frank Bonarens, Patrick Feifel, and Simon Funke. Using ontologies for dataset engineering in automotive ai applications. In *2022 Design, Automation & Test in Europe Conference & Exhibition (DATE)*, pp. 526–531. IEEE, 2022.
- ISO. ISO/PAS 8800:2024 – Road vehicles — Safety and artificial intelligence, 2024. Available at: <https://www.iso.org/standard/83303.html>.
- Saachi Jain, Hannah Lawrence, Ankur Moitra, and Aleksander Madry. Distilling model failures as directions in latent space. In *The Eleventh International Conference on Learning Representations*, 2023. URL <https://openreview.net/forum?id=99RpBVpLiX>.
- Siwon Kim, Jinoh Oh, Sungjin Lee, Seunghak Yu, Jaeyoung Do, and Tara Taghavi. Grounding counterfactual explanation of image classifiers to textual concept space. In *Proceedings of the IEEE/CVF Conference on Computer Vision and Pattern Recognition*, pp. 10942–10950, 2023.
- Philip Koopman and Frank Fratrick. How many operational design domains, objects, and events? In *SafeAI@AAAI*, 2019.
- Satyapriya Krishna, Tessa Han, Alex Gu, Javin Pombra, Shahin Jabbari, Steven Wu, and Himabindu Lakkaraju. The disagreement problem in explainable machine learning: A practitioner’s perspective. *arXiv preprint arXiv:2202.01602*, 2022.
- Xinyue Li, Zhenpeng Chen, Jie M Zhang, Federica Sarro, Ying Zhang, and Xuanzhe Liu. Dark-skin individuals are at more risk on the street: Unmasking fairness issues of autonomous driving systems. *arXiv preprint arXiv:2308.02935*, 2023.
- Yanwei Li, Hengshuang Zhao, Xiaojuan Qi, Liwei Wang, Zeming Li, Jian Sun, and Jiaya Jia. Fully convolutional networks for panoptic segmentation. In *Proceedings of the IEEE/CVF conference on computer vision and pattern recognition*, pp. 214–223, 2021.

- 
- Zhuang Liu, Hanzi Mao, Chao-Yuan Wu, Christoph Feichtenhofer, Trevor Darrell, and Saining Xie. A convnet for the 2020s. In *Proceedings of the IEEE/CVF conference on computer vision and pattern recognition*, pp. 11976–11986, 2022.
- Ziwei Liu, Ping Luo, Xiaogang Wang, and Xiaoou Tang. Deep learning face attributes in the wild. In *Proceedings of International Conference on Computer Vision (ICCV)*, December 2015.
- Scott M Lundberg and Su-In Lee. A unified approach to interpreting model predictions. *Advances in neural information processing systems*, 30, 2017.
- Usman Mahmood, Robik Shrestha, David DB Bates, Lorenzo Mannelli, Giuseppe Corrias, Yusuf Emre Erdi, and Christopher Kanan. Detecting spurious correlations with sanity tests for artificial intelligence guided radiology systems. *Frontiers in digital health*, 3:671015, 2021.
- Jan Hendrik Metzen, Robin Huttmacher, N. Grace Hua, Valentyn Boreiko, and Dan Zhang. Identification of systematic errors of image classifiers on rare subgroups. In *Proceedings of the IEEE/CVF International Conference on Computer Vision (ICCV)*, pp. 5064–5073, October 2023.
- George A Miller. Wordnet: a lexical database for english. *Communications of the ACM*, 38(11):39–41, 1995.
- Curtis Northcutt, Lu Jiang, and Isaac Chuang. Confident learning: Estimating uncertainty in dataset labels. *Journal of Artificial Intelligence Research*, 70:1373–1411, 2021.
- Luke Oakden-Rayner, Jared Dunnmon, Gustavo Carneiro, and Christopher Ré. Hidden stratification causes clinically meaningful failures in machine learning for medical imaging. In *Proceedings of the ACM conference on health, inference, and learning*, pp. 151–159, 2020.
- Gregory Plumb, Nari Johnson, Angel Cabrera, and Ameet Talwalkar. Towards a more rigorous science of blindspot discovery in image classification models. *Transactions on Machine Learning Research*, 2023. ISSN 2835-8856. URL <https://openreview.net/forum?id=MaDvbLaBiF>. Expert Certification.
- Alec Radford, Jong Wook Kim, Chris Hallacy, Aditya Ramesh, Gabriel Goh, Sandhini Agarwal, Girish Sastry, Amanda Askell, Pamela Mishkin, Jack Clark, et al. Learning transferable visual models from natural language supervision. In *International Conference on Machine Learning*, pp. 8748–8763. PMLR, 2021.
- Shaoqing Ren, Kaiming He, Ross Girshick, and Jian Sun. Faster r-cnn: Towards real-time object detection with region proposal networks. *Advances in neural information processing systems*, 28, 2015.
- Marco Tulio Ribeiro, Sameer Singh, and Carlos Guestrin. "why should i trust you?" explaining the predictions of any classifier. In *Proceedings of the 22nd ACM SIGKDD international conference on knowledge discovery and data mining*, pp. 1135–1144, 2016.
- Tal Ridnik, Emanuel Ben-Baruch, Asaf Noy, and Lihi Zelnik-Manor. Imagenet-21k pretraining for the masses. *arXiv preprint arXiv:2104.10972*, 2021.
- Olga Russakovsky, Jia Deng, Hao Su, Jonathan Krause, Sanjeev Satheesh, Sean Ma, Zhiheng Huang, Andrej Karpathy, Aditya Khosla, Michael Bernstein, et al. Imagenet large scale visual recognition challenge. *International journal of computer vision*, 115:211–252, 2015.
- Svetlana Sagadeeva and Matthias Boehm. Sliceline: Fast, linear-algebra-based slice finding for ml model debugging. In *Proceedings of the 2021 International Conference on Management of Data*, pp. 2290–2299, 2021.
- Shiori Sagawa, Pang Wei Koh, Tatsunori B Hashimoto, and Percy Liang. Distributionally robust neural networks for group shifts: On the importance of regularization for worst-case generalization. *arXiv preprint arXiv:1911.08731*, 2019.
- Shibani Santurkar, Dimitris Tsipras, and Aleksander Madry. Breeds: Benchmarks for subpopulation shift. *arXiv preprint arXiv:2008.04859*, 2020.



- 
- Vaishaal Shankar, Rebecca Roelofs, Horia Mania, Alex Fang, Benjamin Recht, and Ludwig Schmidt. Evaluating machine accuracy on imagenet. In *International Conference on Machine Learning*, pp. 8634–8644. PMLR, 2020.
- Eric Slyman, Minsuk Kahng, and Stefan Lee. Vlslice: Interactive vision-and-language slice discovery. In *Proceedings of the IEEE/CVF International Conference on Computer Vision*, pp. 15291–15301, 2023.
- Zeyu Wang, Klint Qinami, Ioannis Christos Karakozis, Kyle Genova, Prem Nair, Kenji Hata, and Olga Russakovsky. Towards fairness in visual recognition: Effective strategies for bias mitigation. In *Proceedings of the IEEE/CVF conference on computer vision and pattern recognition*, pp. 8919–8928, 2020.
- Olivia Wiles, Isabela Albuquerque, and Sven Gowal. Discovering bugs in vision models using off-the-shelf image generation and captioning. In *NeurIPS ML Safety Workshop, 2022*. URL [https://openreview.net/forum?id=maBZZ\\_W01D](https://openreview.net/forum?id=maBZZ_W01D).
- Kai Xiao, Logan Engstrom, Andrew Ilyas, and Aleksander Madry. Noise or signal: The role of image backgrounds in object recognition. *arXiv preprint arXiv:2006.09994*, 2020.
- Fisher Yu, Haofeng Chen, Xin Wang, Wenqi Xian, Yingying Chen, Fangchen Liu, Vashisht Madhavan, and Trevor Darrell. Bdd100k: A diverse driving dataset for heterogeneous multitask learning. In *Proceedings of the IEEE/CVF conference on computer vision and pattern recognition*, pp. 2636–2645, 2020.
- Marc Zeller, Thomas Waschulzik, Martin Rothfelder, and Cornel Klein. Safety assurance of a driverless regional train-insight in the safe. train project. In *2023 IEEE 34th International Symposium on Software Reliability Engineering Workshops (ISSREW)*, pp. 41–42. IEEE, 2023.
- Oliver Zendel, Markus Murschitz, Marcel Zeilinger, Daniel Steininger, Sara Abbasi, and Csaba Beleznai. Railsem19: A dataset for semantic rail scene understanding. In *Proceedings of the IEEE/CVF Conference on Computer Vision and Pattern Recognition (CVPR) Workshops*, June 2019.
- Sixiao Zheng, Jiachen Lu, Hengshuang Zhao, Xiatian Zhu, Zekun Luo, Yabiao Wang, Yanwei Fu, Jianfeng Feng, Tao Xiang, Philip HS Torr, et al. Rethinking semantic segmentation from a sequence-to-sequence perspective with transformers. In *Proceedings of the IEEE/CVF conference on computer vision and pattern recognition*, pp. 6881–6890, 2021.

---

# Appendix

## A Datasets, DNNs, Hyperparameters

**Datasets:** We use four datasets in our experiments to test different black-box DNNs-under-test. First, as a proof-of-concept for our overall approach, we use the CelebA Liu et al. (2015) dataset with a rich collection of 40 facial attributes (metadata) for 202 599 images of celebrity faces. We use the aligned PNG images provided by the authors, which are at a resolution of  $178 \times 218$  pixels. Next, for the pedestrian detection tasks, we consider BDD100k Yu et al. (2020), Cityscapes Cordts et al. (2016), and RailSem19 Zendel et al. (2019). In these datasets, we focus only on the pedestrian class in the 2D-bounding box and semantic segmentation tasks. For BDD100k, we consider the predefined validation set of 10k samples of resolution  $1280 \times 720$ , while in Cityscapes and RailSem19, due to their smaller dataset sizes, we use the entire train and validation sets containing 3475 (test set is not considered due to lack of GT) and 8500 samples with image resolutions  $2048 \times 1024$  and  $1920 \times 1080$  respectively.

**Models (DNNs-under-test):** We evaluate four black-box models for ODD aligned systematic weaknesses. For the first experiment, we consider the publicly available ViT-B-16 Dosovitskiy et al. (2020) model pre-trained on ImageNet21k Ridnik et al. (2021) from the python library timm.<sup>11</sup> Second, we use the pre-trained publicly available Faster R-CNN Ren et al. (2015) object detector with ConvNeXt-T Liu et al. (2022) backbone. The model weights are available on the BDD100k model Zoo.<sup>12</sup> Third, for the Cityscapes dataset, we use a pre-trained SETR PUP Zheng et al. (2021) semantic segmentation model. The model weights are available on the mmsegmentation codebase.<sup>13</sup> Finally, from the railway domain, we use a PanopticFCN Li et al. (2021) model, which has been trained by an industrial partner on a large proprietary dataset also including RailSem19 Zendel et al. (2019). We consider this as a complete black box and have no details on the concrete training. For the autonomous datasets, the black-box model performance per object (i.e., pedestrian) is measured by the intersection-over-union (IoU).

**Parameters of CLIP and SliceLine:** For the metadata generation, we use a pre-trained CLIP Radford et al. (2021) with image encoder (ViT-L/14 Dosovitskiy et al. (2020)). For SliceLine, we use a python implementation<sup>14</sup> and choose default  $\alpha$  and  $\sigma$  values of 0.95 and  $n/100$  where  $n$  defines the size of the structured data as proposed in Sagadeeva & Boehm (2021). We run the experiments for a depth level of 2, cut-off of  $1.5 * \bar{e}|_S$  (except when evaluating PanopticFCN where use  $1 * \bar{e}|_S$ ) and present the top-5 weak slices for AD experiments. For synthetic data experiment, we incrementally increase k from 1 to 60.

## B Synthetic Data Generation Parameters

The purpose of the synthetic data experiment is to evaluate the proposed workflow with control over the quality of labelling and without influence of correlations. Therefore, we build a tabular dataset with 9 “real” semantic dimensions ( $dim_1, \dots, dim_9$ ) containing 200,000 rows. For each of these dimensions, we generate a synthetic dimension as a proxy for labelling by CLIP. All dimensions contain binary attributes. For the first five dimensions, the distribution of true attribute is imbalanced, i.e., only 5% of overall samples ([8000, 9000, 10000, 11000, 12000]) respectively. The other dimensions are balanced between both attributes. A final column contains errors simulating the **DuT** performance. Next, we define a set of slices and induce errors for each of the slices. For our experiments, we induce the following errors:  $\{dim_1: 0.19, dim_2 \& dim_3: 0.18, dim_4: 0.23, dim_5: 0.3, dim_6: 0.07, dim_7: 0.04, dim_8: 0.01, dim_9: 0.02\}$ . As we have 100 runs for different labelling qualities, we introduce random fluctuations between -0.01 and 0.01 to these error values. The choice of errors and number of dimensions is to align the synthetic data with the celebA experiment and also to effectively induce errors. If all dimensions would contribute roughly equally to the error rate, no strong signal for a specific slice, in contrast to the others, could be found. We generate 100 runs each for 3 different labelling qualities. That is, we generate the “observed” metadata from the “real”

---

<sup>11</sup><https://github.com/huggingface/pytorch-image-models>

<sup>12</sup><https://github.com/SysCV/bdd100k-models/tree/main/det>

<sup>13</sup><https://github.com/open-mmlab/mmdetection>

<sup>14</sup><https://github.com/DataDome/sliceline>

one using a random pre-defined “precision” value. For good quality, this precision value to detect attribute 1 of each dimension is sampled from a uniform distribution between 0.8 and 1.0. For attribute 0, we sample between 0.8 and 1.0. For medium quality and attribute 1, we sample from 0.4 and 0.6 and for attribute 0 between 0.4 and 0.7. For bad quality, for attribute 1, we sample between 0.1 and 0.4 and for attribute 0 between 0.3 and 0.6.

## C Human-understandable Dimensions

Herrmann et al. (2022) have proposed ontologies for different dynamic objects (e.g., pedestrians) to build ODDs for AD vehicles. While these proposed ontologies do not yet completely capture all safety-relevant features, they provide a reference to the direction safety experts intend to take to build evidences for safety augmentations of AD vehicles. To enable such evidence formulation, we perform our experiments on a subset of the concepts discussed in these ontologies as shown in tables 5 and 6. In the case of BDD100k, as information about occlusion is provided in the dataset, we combine our generated metadata with this additional information. For the CelebA experiment, as the input distribution is not directly related to the AD domain, we consider semantic concepts that are more suitable for this dataset as shown in table 5. Similar to Gannamaneni et al. (2023), we encode the input image using the CLIP image encoder. For celebA, we encode the whole input image, while for the AD experiments, we encode individual pedestrian crops as a single input. We consider each semantic dimension and its corresponding attributes to generate metadata for an input image.

| Semantic dimension | Attributes |        |
|--------------------|------------|--------|
| Gender             | Male       | Female |
| Skin color         | Light      | Dark   |
| Age                | Young      | Adult  |
| Beard              | True       | False  |
| Goatee             | True       | False  |
| Bald               | True       | False  |
| Wearing-Hat        | True       | False  |
| Wearing-Eyeglasses | True       | False  |
| Smiling            | True       | False  |

Table 5: The ODD used for the celebA experiment. The first column represents the different semantic dimensions (in analogy to safety-relevant features). For each dimension, different attributes are considered and generated as metadata using our metadata generation process.

## D SliceLine Workflow

SliceLine works on the individual errors  $e_i$  of data samples  $i$ . These, in the original work, can be defined as  $e_i = 1 - p_i$  with the DuT predicted probability  $p_i$  for the correct class. In the remainder, we make the simplifying assumption that  $e_i \in \{0, 1\}$  indicates whether  $i$  was classified correctly,  $e_i = 0$ , or not,  $e_i = 1$ . The workflow of SliceLine to identify weak slices is as follows: Initially, for depth level 1, a breadth search over all attributes in the metadata is performed such that only single features form a slice (e.g., a slice containing all data points with condition ( $gender : male$ )). Checks are performed over these slices to ensure thresholds are met (e.g., minimum slice size specified via some parameter  $\sigma$ ). Next, based on the slice scores from eq. (5), the slices are ordered, and a list of top-k weak slices is populated. The hyperparameter  $\alpha$  in eq. (5) allows us to weight the size of the slice as well as the error signal. At depth level 2 and above, combinations of two attributes are chosen to form a slice (e.g., slice containing all data points with condition ( $gender = male$ )&(occlusion = (0.9, 1.0])). The list of weak slices is updated after each depth level. The maximum depth level is a hyperparameter. In addition, pruning steps are also performed at each depth level. The conditions for pruning have a monotonicity property, which ensures that all potential sub-slices of a pruned slice would also fulfil the pruning condition. Once the maximum depth level has been reached, the algorithm terminates, and the final list of top-k weak slices are available.

| Semantic dimension               | Attributes   |            |
|----------------------------------|--|------------|
| Gender                           | Male   | Female     |
| Skin color                       | White  | Dark       |
| Age                              | Young  | Adult      |
| Clothing color                   | Bright-color   | Dark-color |
| Blurry                           | True   | False      |
| Occlusion <sup>†</sup>           | True   | False      |
| Construction-worker <sup>‡</sup> | True   | False      |
| Size                             | 10 quantile binned values of bounding box pixel area |            |

Table 6: A sample ontology for pedestrians used in our AD dataset experiments. The first column represents the different semantic dimensions (safety relevant features). For each dimension, different attributes are considered and generated as metadata using our metadata generation process. Metadata that is generated from CLIP but from available through other sources (e.g., GT) is not considered noisy and, therefore, we do not perform precision and recall estimation by human sampling. <sup>†</sup> Occlusion is available as GT from the BDD100k dataset and we only consider it in corresponding experiment. <sup>‡</sup> RailSem19 dataset contains several images where construction-workers are present near railway tracks. Therefore, we additionally consider this dimension for CLIP labelling to identify if models have weaknesses identifying construction workers. Size of pedestrian is estimated by calculating product of bounding width and height.

$$\text{Scoring Function}(\mathcal{S}) = \alpha \frac{e|\mathcal{S} - e|_{\mathcal{D}}}{e|_{\mathcal{D}}} - (1 - \alpha) \frac{|\mathcal{D}| - |\mathcal{S}|}{|\mathcal{S}|} \quad (5)$$

## E Derivation of $p(e|\mathcal{C})$ and $p(e|\mathcal{S})$

To derive eq. (2) and eq. (1) from section 3, we first consider the joined probability  $p(e, \mathcal{C}, \mathcal{S})$ , where  $e$  denotes the DuT error,  $\mathcal{C}$  the labelling, and  $\mathcal{S}$  the ground truth for some semantic attribute. Using Bayes' Theorem we can rewrite this as

$$p(e, \mathcal{C}, \mathcal{S}) = p(e|\mathcal{C}, \mathcal{S})p(\mathcal{C}, \mathcal{S}) = p(e|\mathcal{C}, \mathcal{S})p(\mathcal{C}|\mathcal{S})p(\mathcal{S}). \quad (6)$$

Looking additionally at marginal distributions

$$p(e, \mathcal{S}) = \sum_{\mathcal{C}} p(e, \mathcal{C}, \mathcal{S}) = p(\mathcal{S}) \sum_{\mathcal{C}} p(e|\mathcal{C}, \mathcal{S})p(\mathcal{C}|\mathcal{S}), \quad (7)$$

where the sum goes ver all possible values  $\mathcal{C}$  can take, we can write the conditional error probability (or rate if considered over finite data) as

$$p(e|\mathcal{S}) = \sum_{\mathcal{C}} p(e|\mathcal{C}, \mathcal{S})p(\mathcal{C}|\mathcal{S}). \quad (8)$$

At this point, using that  $\mathcal{C}$  takes only binary values, which, for brevity, we denote as  $\mathcal{C}$  if the attribute was detected and as  $-\mathcal{C}$  else,<sup>15</sup> we can expand the sum:

$$p(e|\mathcal{S}) = p(e|\mathcal{C}, \mathcal{S})p(\mathcal{C}|\mathcal{S}) + p(e|-\mathcal{C}, \mathcal{S})p(-\mathcal{C}|\mathcal{S}). \quad (9)$$

Within this expression, we can identify the recall

$$r_{\mathcal{C}} \equiv p(\mathcal{C}|\mathcal{S}) \quad (10)$$

of the labelling method, that is the probability we will obtain correct identification of the semantic attribute given its presence. Using further the normalisation property

$$1 = \sum_{\mathcal{C}} p(\mathcal{C}|\mathcal{S}) \quad \rightarrow \quad p(-\mathcal{C}|\mathcal{S}) = 1 - p(\mathcal{C}|\mathcal{S}), \quad (11)$$

<sup>15</sup>This is a slight over-use of the notation, but it is apparent from context whether  $\mathcal{C}$  is meant as the random variable for the labelling, or as its value in the sense of positive detection.

we arrive at the originally presented eq. (1):

$$p(e|\mathcal{S}) = r_c p(e|\mathcal{C}, \mathcal{S}) + (1 - r_c) p(e|\neg\mathcal{C}, \mathcal{S}). \quad (12)$$

Along the same lines eq. (2),

$$p(e|\mathcal{C}) \equiv p_c p(e|\mathcal{C}, \mathcal{S}) + (1 - p_c) p(e|\mathcal{C}, \neg\mathcal{S}), \quad (13)$$

can be derived, however with the identification

$$p_c = p(\mathcal{S}|\mathcal{C}), \quad (14)$$

i.e., the precision of the labelling process.

## F Derivation of Correction Equation

As discussed in section 3, the annotation process may not be a perfect process. Furthermore, there is no guarantee that the failure modes within this process do not overlap the failures of **DuT**, i.e., there is a possibility that some amount of correlation could exist between the errors of annotation process and the errors of **DuT**. Therefore, we frame this using the following

$$\delta p(e|\mathcal{S}) = p(e|\neg\mathcal{C}, \mathcal{S}) - p(e|\mathcal{C}, \mathcal{S}) \quad (15)$$

By considering earlier equations and their complementary forms for  $\neg\mathcal{S}$  and reducing the equation set, we obtain

$$A = \begin{pmatrix} p_c & 1 - p_c \\ 1 - p_{-c} & p_{-c} \end{pmatrix}, \quad B = \begin{pmatrix} p(e|\mathcal{C}) + (p_c) \delta p(e|\neg\mathcal{S}) \\ p(e|\neg\mathcal{C}) + (p_{-c}) \delta p(e|\mathcal{S}) \end{pmatrix},$$

$$A \begin{pmatrix} p(e|\mathcal{C}, \mathcal{S}) \\ p(e|\neg\mathcal{C}, \neg\mathcal{S}) \end{pmatrix} = B$$

Here, the  $\det(A)$  is given by  $p_c + p_{-c} - 1$  and inverse of  $A$  is given by

$$A^{-1} = \frac{1}{p_c + p_{-c} - 1} \begin{pmatrix} p_{-c} & -(1 - p_c) \\ -(1 - p_{-c}) & p_c \end{pmatrix}. \quad (16)$$

Solving for the intermediate value of  $p(e|\neg\mathcal{C}, \mathcal{S})$  and plugging this in eq. (12) along with eq. (15), we obtain the final equation

$$p(e|\mathcal{S}) = \underbrace{\frac{p(e|\mathcal{C}) p_{-c} + p(e|\neg\mathcal{C}) (p_c - 1)}{p_c + p_{-c} - 1}}_{\text{hypothesis}} + \underbrace{\delta p(e|\mathcal{S}) \left( \frac{p_c p_{-c}}{p_c + p_{-c} - 1} - r_c \right)}_{\text{correction terms}} + \delta p(e|\neg\mathcal{S}) \frac{(p_c - 1) p_{-c}}{p_c + p_{-c} - 1}. \quad (17)$$

Regarding the denominator  $p_c + p_{-c} - 1$ , it can be zero (or approximately zero) for some combinations of precision of the metadata annotation process. In these cases, no statement can be made on  $\mathcal{S}$  as the performance of the annotation classification does not allow separation of  $\mathcal{S}$  from the rest of the data and any observable error differences on  $\mathcal{C}$  potentially stems only from the correction factors. Besides this technical breakdown of the hypothesis, it should be pointed out that the scaling factors  $\kappa_{\mathcal{S}, \neg\mathcal{S}}$  depend only on the performance of the annotation process and thus can be determined without knowing the correction factors  $\delta p$  themselves. While the latter are challenging to determine in practice they are rarely non-zero, even in cases where the hypothesis holds, due to fluctuations (e.g. when errors are determined on finite sample sizes). Knowing the magnitude of  $\kappa$  therefore allows us a degree of certainty on the statements of the hypothesis.

## G Quantitative Evaluation of Metadata Generation Process

Our metadata generation is a form of data labelling process. Within this work, we chose CLIP Radford et al. (2021) to generate the metadata but know that for certain attributes of the ODDs the performance might be far below human capabilities, compare, e.g., Gannamaneni et al. (2023). To estimate the performance of our metadata generation process without large-scale evaluation or manual labelling, we take a simplifying view. For each slice  $\mathcal{C}$  containing a semantic concept identified by CLIP, for instance, images containing gender “female”, we randomly draw a few samples to create a smaller subset  $\mathcal{R}$ . Let  $q$  denote the probability that images within  $\mathcal{C}$  contain the correct semantic concept. By manually evaluating the smaller sample of images  $\mathcal{R} \subset \mathcal{C}$  (drawn with replacement), we can model the posterior distribution for  $q$  using Bayes theorem, that is

$$p(q|\mathcal{R}) = \frac{p(q)p(\mathcal{R}|q)}{p(\mathcal{R})} \propto p(\mathcal{R}|q). \quad (18)$$

Therein, we assumed a flat prior, i.e.  $p(q) = \text{const.}$ . The probability of the observed sample  $\mathcal{R}$  is given by

$$p(\mathcal{R}|q) = \binom{n}{k} q^k (1-q)^{n-k}, \quad (19)$$

where  $n = |\mathcal{R}|$  is the size of the observed sample taken from  $\mathcal{S}$  and  $k \leq n$  is the number of observed positive, i.e., correct instances. The true value for  $q$  for the entire slice would describe the precision of the labelling of the concept as it is the ratio of true instances to the overall number of samples. We can approximate it using the small set using

$$p_{\text{precision}}(q|\mathcal{R}) = \frac{(n+1)!}{k!(n-k)!} q^k (1-q)^{n-k}, \quad (20)$$

where the factorials serve as the normalisation. Using eq. (20), we can, therefore, determine both the expected value of  $q$  as well as our uncertainty of its value, which we report in terms of the standard deviation  $\sigma$ . As a side note, for values of  $q$  near 0 or 1, the Binomial distribution is asymmetric and the standard deviation is not always a faithful measure of “true” deviation. However, we compared with a quantile based approach, taking the range from the 1/6<sup>th</sup> to 5/6<sup>th</sup> quantile, and found only minor discrepancies.

Besides estimating the precision, we are also interested in estimating the recall of the labelling process. This latter quantity is harder to evaluate as it depends both on the number of true positives and false negatives. Let  $P$  and  $N$  denote the total number of data points that are classified as containing, or respectively, as not containing, the semantic concept. Then the probability over the total number of true positives is given by  $p_{\text{precision}}(q|\mathcal{R}_P)$ , where  $\mathcal{R}_P$  is a random sample taken from the set  $\mathcal{C}_P$  of positively classified elements. A similar statement holds for the number of false negatives, where a sample  $\mathcal{R}_N$  from the non-detected set can be used. However, in this case, we either have to count (for  $k$ ) the number of prediction errors or use the inverse outcome  $1 - q$ . Given that both samples are free of intersection, that is  $\mathcal{R}_P \cap \mathcal{R}_N = \emptyset$ , we make the assumption that the obtained probabilities  $q_P$  and  $q_N$  are independent from one another. In this case, we can formulate the recall as

$$\begin{aligned} p_{\text{recall}}(q|\mathcal{R}_P, \mathcal{R}_N) &= \int_0^1 dq_P \int_0^1 dq_N \\ &\times \delta\left(q - \frac{Pq_P}{Pq_P + N(1-q_N)}\right) \\ &\times p_{\text{precision}}(q_P|\mathcal{R}_P) p_{\text{precision}}(q_N|\mathcal{R}_N), \end{aligned} \quad (21)$$

where we interpret  $p_{\text{precision}}$  such that in both cases correct predictions are counted while  $\delta$  denotes a Dirac-Delta Distribution. We evaluate this function numerically and use the results of  $p_{\text{recall}}$  in the same way as for the precision above regarding, e.g., the reported standard deviation.

## H Precision Sampling at different levels

In appendix G, we provide the framework on how precision and recall can be estimated by sampling data in slices. In this section, we present the concrete steps taken at level 1 to operationalize it and also steps taken

---

to calculate precision and recall at higher levels. At level 1, in synthetic and celebA experiments, as GT labels are available in addition to classification function  $\mathcal{G}$  labels, human evaluation of slices is not necessary. For each slice in data, before running SliceLine, we sample with replacement ( $n=60$ ), and using GT slice labels, calculate precision and recall based on appendix G. This gives us mean and standard deviations of precision and recall which can be used with eq. (4). For AD datasets, as GT labels are not available, we perform human evaluation by first taking 60 samples for each level 1 slice. The results of this are shown in table 3.

At level 2 and higher, human sampling of precisions gets very labour-intensive even if considering only 9 semantic dimensions with binary attributes. Therefore, we incorporate the parent-level precisions calculated earlier to estimate corrected errors by accounting for their contributions. This approach extends the binary case discussed in eq. (16) to a multi-class setting. From level 2 onward, we construct a composite inverse matrix, similar to the one in eq. (16), and apply it to the observed errors. This transformation yields the corrected errors for each combination..

## I Further results: CelebA Evaluations

In the synthetic data experiment, we provide the spread of errors and the precision and recall of slice recovery in comparison to an Oracle for different values of  $k$ . With the GT metadata in the celebA dataset, we build a similar Oracle for comparison and provide similar error spread and precision and recall values of SWD-1,2,3 in fig. 5. Here, the plot depicting spread of errors is restricted to level 1 errors for better visualization. However, the precision and recall plot is based on the full level 2 slices.

## J Evaluation of Top-5 Weak Slices

In this section, we provide both the quantitative and qualitative results of our experiments. For the celebA dataset, figs. 6 to 9 contain the identified top-5 weak slices in the experiments SWD-3, DOMINO, Spotlight, and SVM FD respectively. We provide 8 samples from each of the top-5 slices found by the methods and 8 samples from the remaining data, except SVM FD which only provides 1 weak slice. In addition, we provide four slice descriptions given by DOMINO for each slice and the single slice description of SVM FD. While the actionability of our proposed approach is inherent as the identified weak slices are based on semantic concepts from the ODD, the textual descriptions from DOMINO are comparatively less useful. Furthermore, by focusing only on the samples from DOMINO, it is still hard to identify what semantic concepts uniquely constitute a slice. For example, if we consider an image from the remaining data (rightmost column), it is not straightforward to say if this image belongs to any of the first four weak slices. While the fifth slice does seem to capture a coherent slice, images of sport persons, the  $FNR$  is significantly lower than what is identified by our approach. It is important to note that both DOMINO and SliceLine judge performance in terms of class probabilities, not false negative counts. Therefore, weak slices can have a slightly better performance in terms of  $FNR$  compared to the overall data, as observed for slice 2 found by DOMINO.

In figs. 10 to 12, pedestrian crop samples from the top-5 weak slices obtained via our method for each autonomous driving experiments are provided. The quantitative evaluation of the top-5 slices for the three experiments can be found in tables 7 to 9.

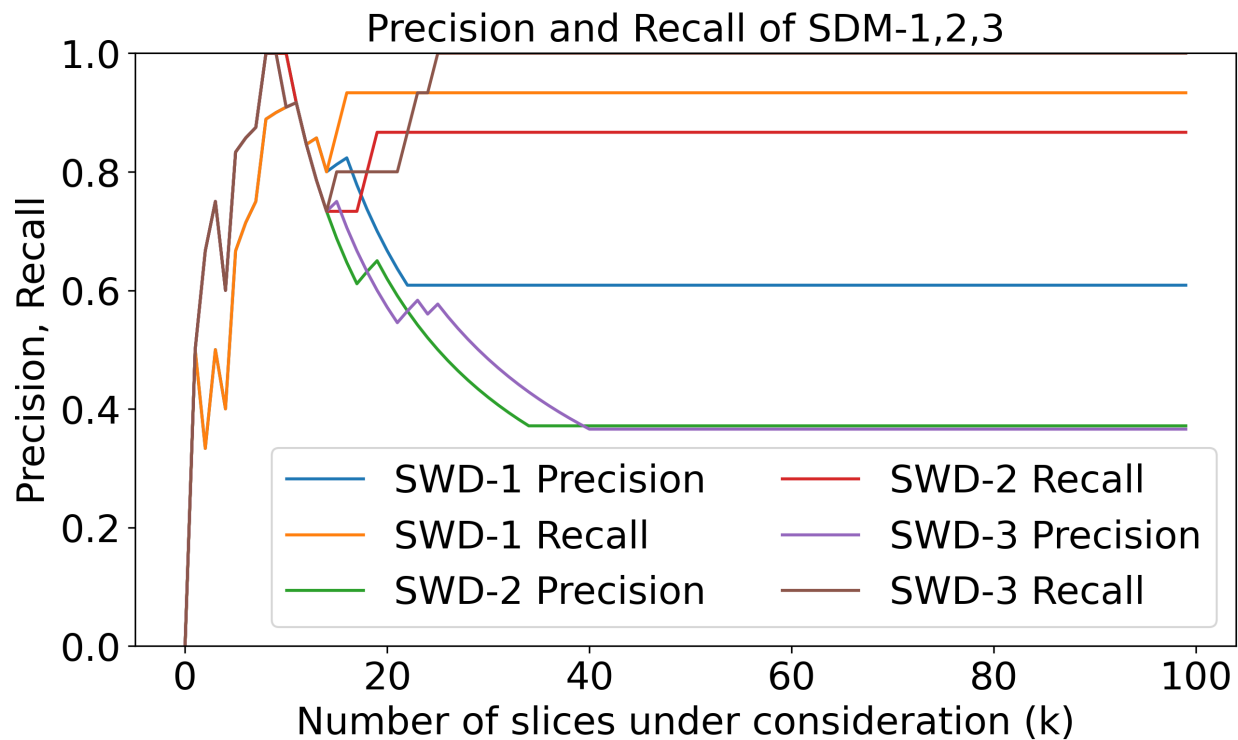
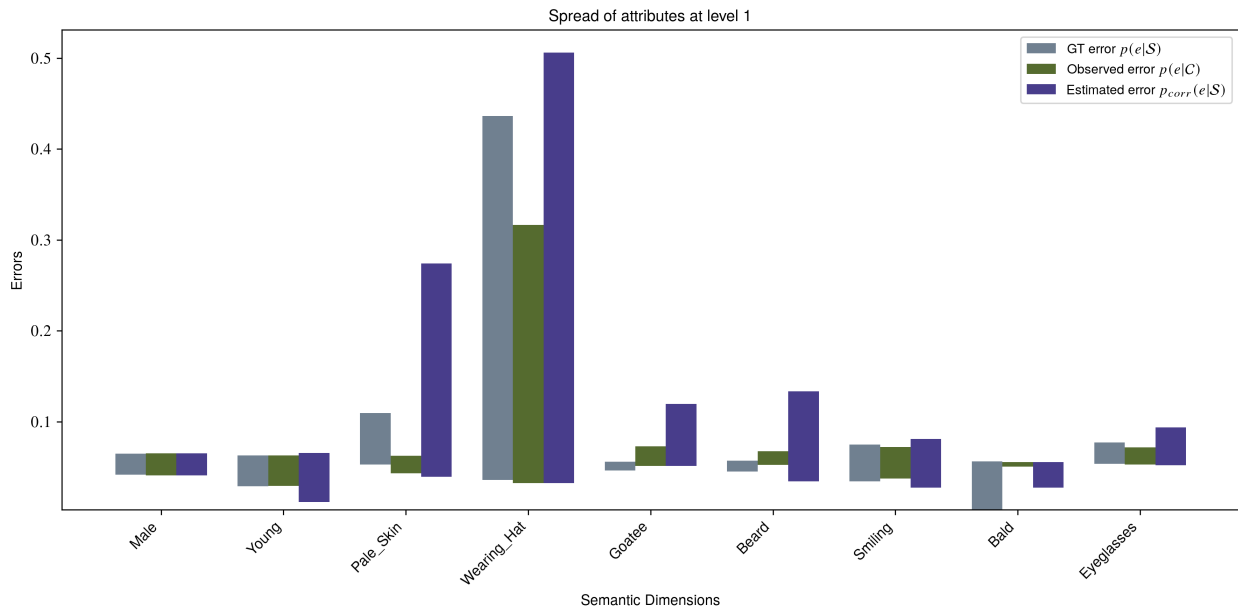


Figure 5: Similar to synthetic data experiment, we provide spread of error (top) and Precision and Recall at different levels of  $k$  for SWD-1,2,3 of algorithm 1 in comparison to the Oracle (bottom). The **DuT** is a ViT-B-16 classification model trained on ImageNet21k and evaluated on celebA dataset. Note that here precision and recall are quality metrics of weak slice discovery and not of labelling quality.



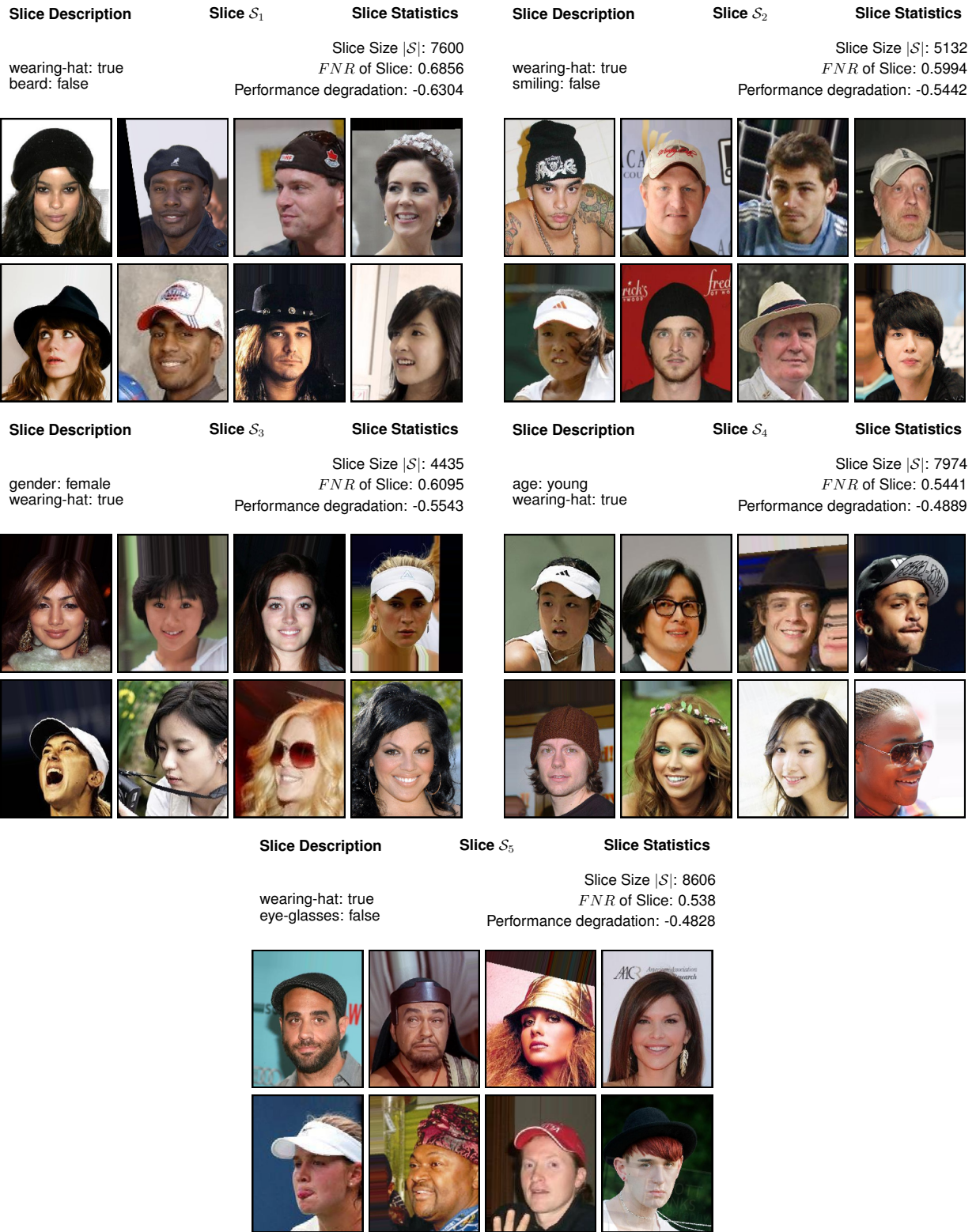


Figure 6: Samples from top-5 weak slices of a ViT-B-16 classification model trained on ImageNet21k and evaluated on the full celebA dataset with metadata generated from CLIP using step 3 in algorithm 1. The statistics provide a quantitative evaluation of the entire slice. For qualitative evaluation, we provide some sample images from the slice.


|                         | Slice 1  | Slice 2  | Slice 3   | Slice 4   | Slice 5   | Remaining Data   |
|-------------------------|--|--|---|---|---|--|
| Slice Size $ S $        | 11726  | 2317   | 3344  | 2565  | 2307  | 180340   |
| $FNR$ of Slice          | 0.6182   | 0.2486   | 0.0499  | 0.1053  | 0.1756  | 0.0146   |
| Performance Degradation | -0.5622  | -0.1926  | 0.0061  | -0.0493   | -0.1196   | 0.0414   |
|                         |    |    |   |    |   |  |
| Slice Descriptions      | <p>“a photo of the vocalist person”</p> <p>“a band photo of a person”</p> <p>“a photo of the choreographer person”</p> <p>“a photo of a person or author.”</p> | <p>“kate moss photo of a person”</p> <p>“a fashion photo of a person”</p> <p>“a photo of a person on runway.”</p> <p>“a photo of a person or model.”</p> | <p>“- bolivia photo of a person”</p> <p>“a photo of a beauty person”</p> <p>“a woman photo of a person”</p> <p>“a photo of a modeling person”</p> | <p>“judy garland photo of a person”</p> <p>“a photo of judy garland person”</p> <p>“a postwar photo of a person”</p> <p>“a photo of a postwar person”</p> | <p>“a photo of a tennis person”</p> <p>“a photo of a person playing tennis.”</p> <p>“a photo of a person playing tennis.”</p> <p>“a photo of a person clinching.”</p> |  |

Figure 7: Samples from top-5 weak slices of a ViT-B-16 classification model trained on ImageNet21k and evaluated on the full celebA dataset (DOMINO). From the 8 samples in each slice, 4 are true positives (green outline) and 4 are false negatives (red outline).

|                         | Slice 1 | Slice 2 | Slice 3 | Slice 4 | Slice 5 | Remaining Data |
|-------------------------|---------|---------|---------|---------|---------|----------------|
| Slice Size $ S $        | 4050    | 3930    | 1873    | 2498    | 3096    | 187152         |
| $FNR$ of Slice          | 0.918   | 0.5542  | 0.6663  | 0.2894  | 0.1925  | 0.0151         |
| Performance Degradation | -0.862  | -0.4982 | -0.6103 | -0.2334 | -0.1365 | 0.0409         |

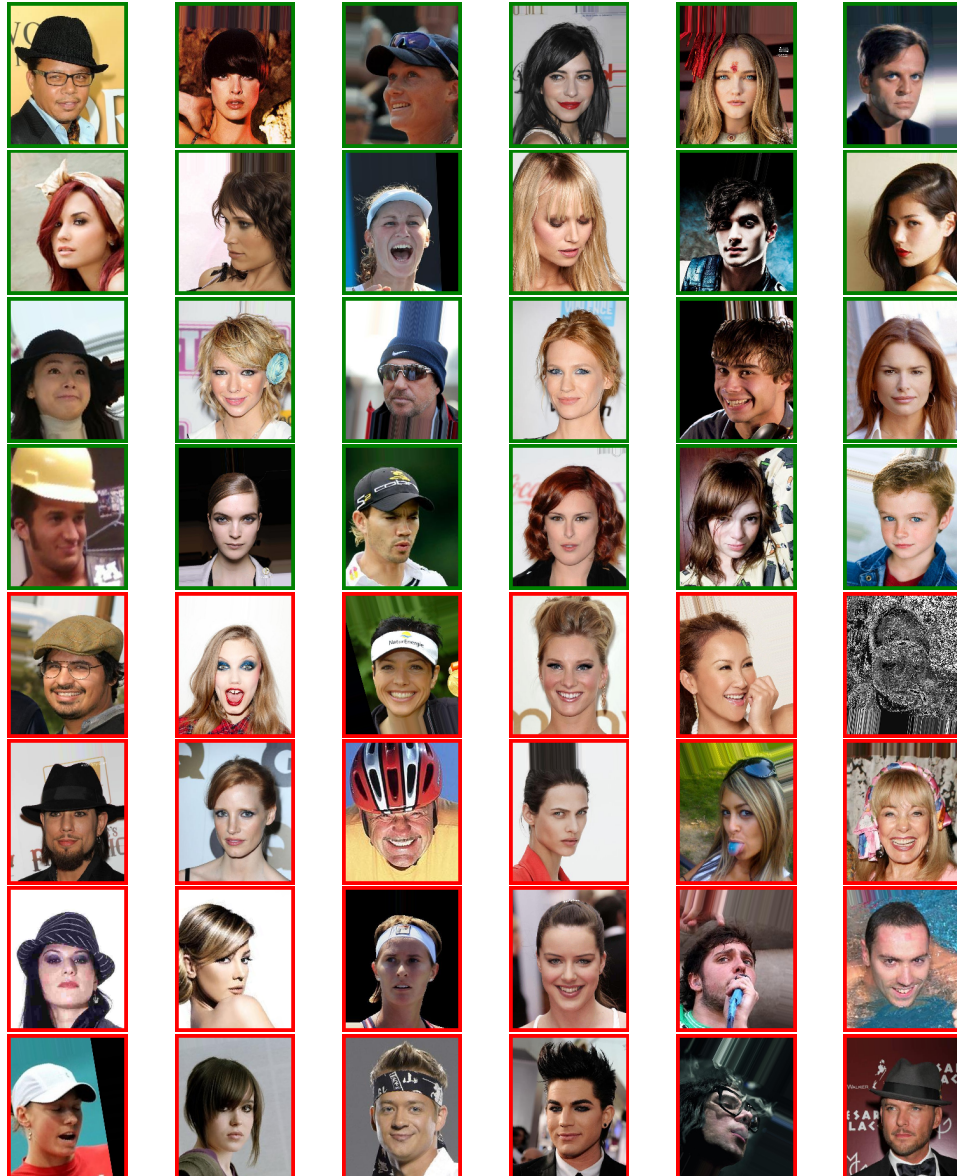


Figure 8: Samples from top-5 weak slices of a ViT-B-16 classification model trained on ImageNet21k and evaluated on the full celebA dataset (Spotlight). From the 8 samples in each slice, 4 are true positives (green outline) and 4 are false negatives (red outline). Spotlight does not provide automatic descriptions of the slices

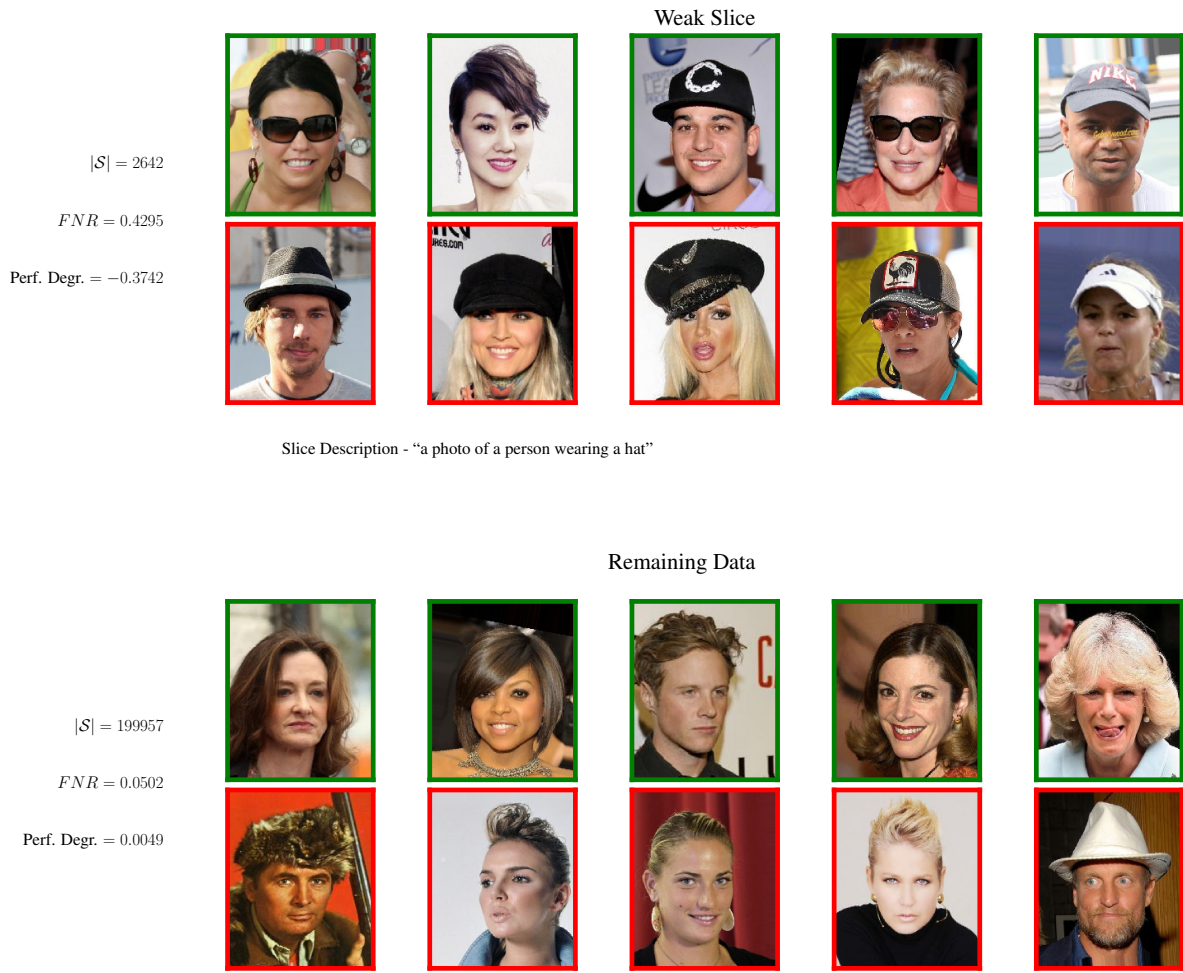


Figure 9: Samples from top-1 weak slices of a ViT-B-16 classification model trained on ImageNet21k and evaluated on the full celebA dataset (SVM-FD). From the 10 samples in each slice, 5 are true positives (green outline) and 5 are false negatives (red outline). SVM-FD only provides one complete weak slice with a description.

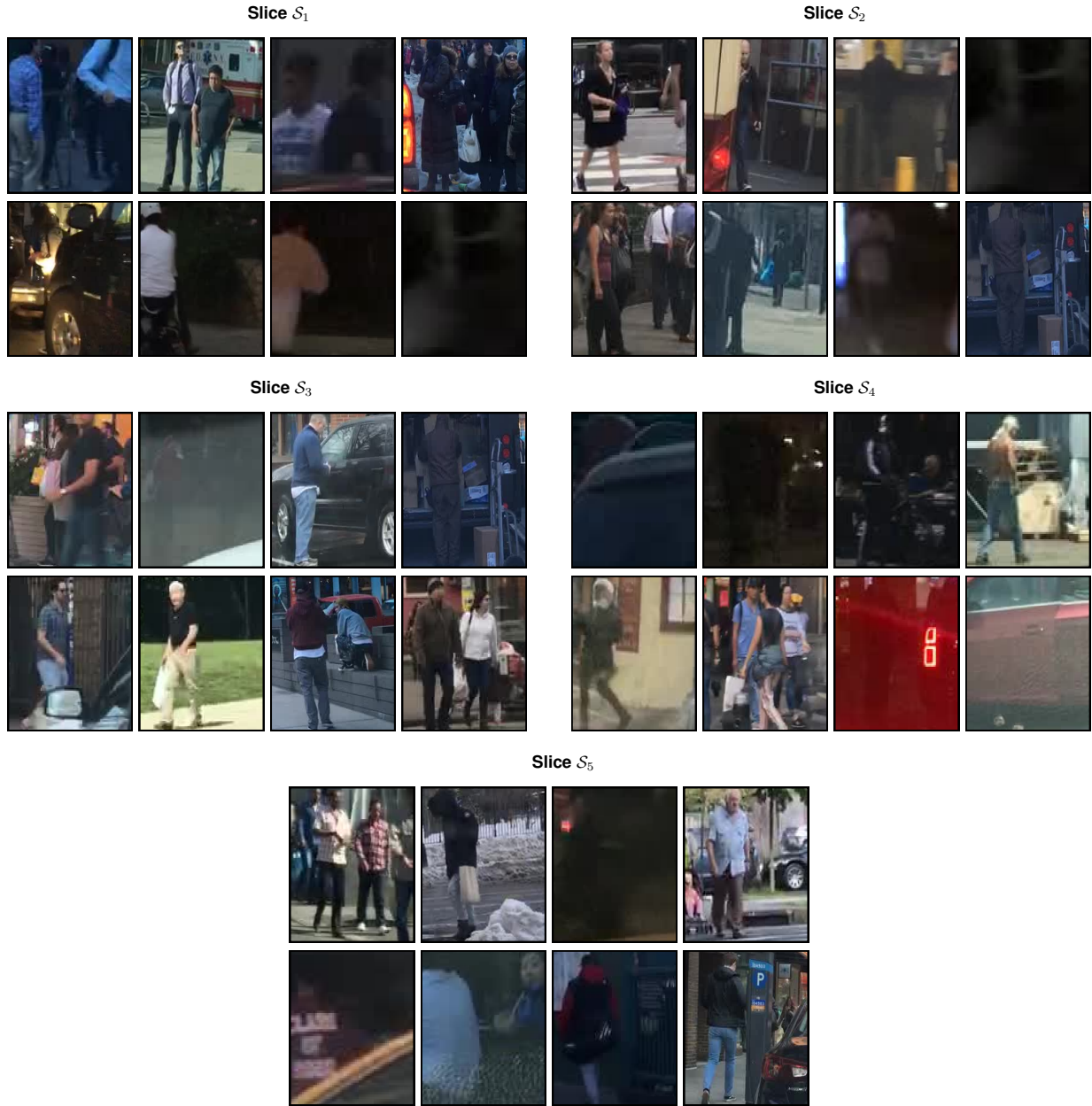


Figure 10: Samples from top-5 weak slices of a Faster R-CNN object detector trained and evaluated on BDD100k dataset.



Figure 11: Samples from top-5 weak slices of a SETR semantic segmentation model trained and evaluated on Cityscapes dataset.

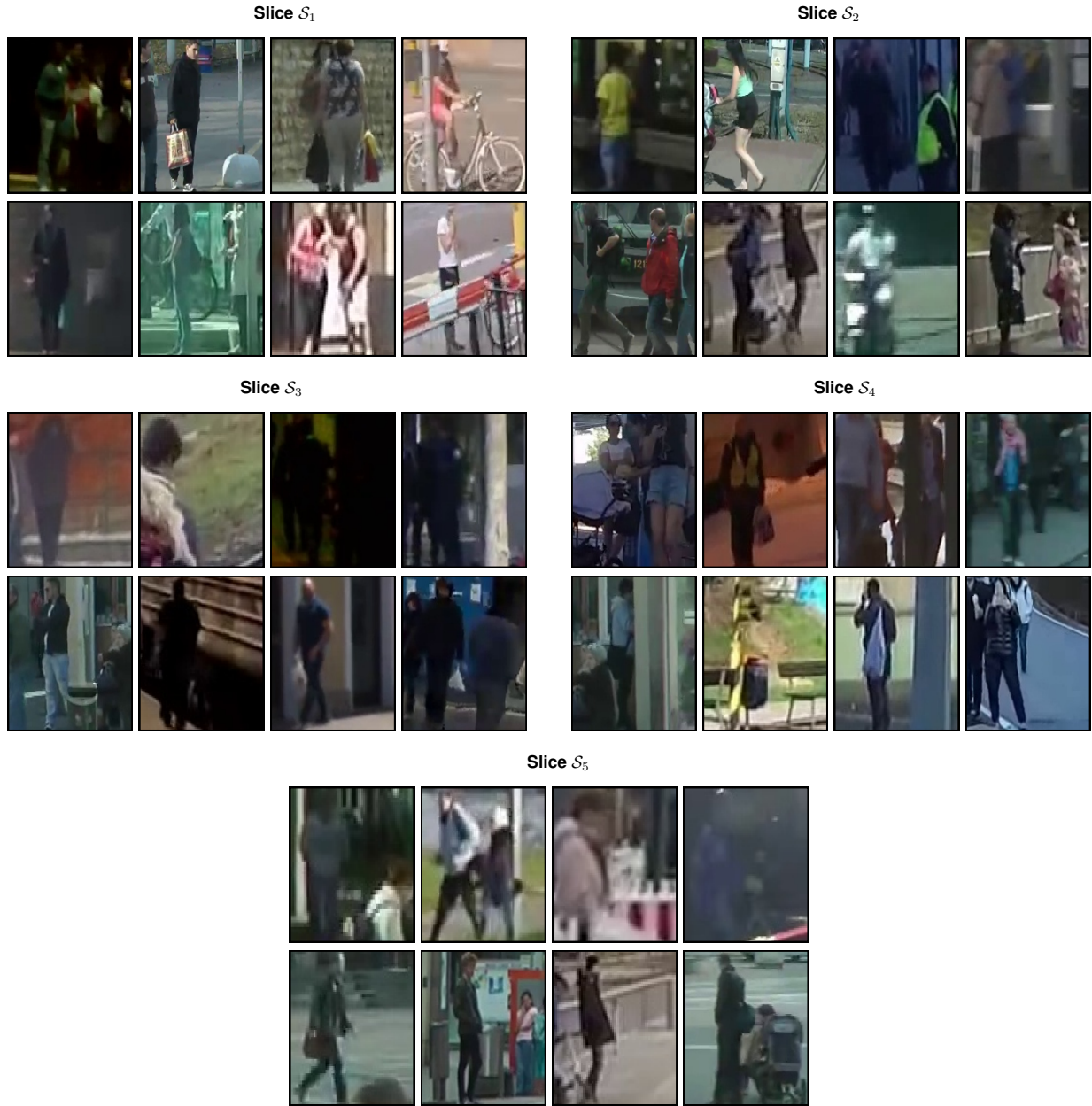


Figure 12: Samples from top-5 weak slices of a Panoptic-FCN model trained and evaluated on RailSem19 dataset. The cut-off threshold is reduced to  $1.0 * \bar{e}|_{\mathcal{S}}$  as  $\bar{e}|_{\mathcal{D}}$  is high in this experiment.

| Slice No.       | $ \mathcal{S} $ | $FNR$  | Avg. Perf.<br>Degra. | Slice Description                                       |
|-----------------|-----------------|--------|----------------------|---|
| $\mathcal{S}_1$ | 319             | 0.2206 | -0.1636              | <b>blurry:</b> false<br><b>occluded:</b> true           |
| $\mathcal{S}_2$ | 508             | 0.2099 | -0.1528              | <b>blurry:</b> false<br><b>cloth.-color:</b> dark-color |
| $\mathcal{S}_3$ | 466             | 0.147  | -0.0899              | <b>blurry:</b> false<br><b>age:</b> adult               |
| $\mathcal{S}_4$ | 773             | 0.1263 | -0.0693              | <b>blurry:</b> false                                    |
| $\mathcal{S}_5$ | 582             | 0.1263 | -0.0693              | <b>blurry:</b> false<br><b>gender:</b> Male             |

Table 7: Quantitative analysis of the top-5 weak slices for the Faster R-CNN object detector trained and evaluated on BDD100k dataset.

| Slice No.       | $ \mathcal{S} $ | $FNR$  | Avg. Perf.<br>Degra. | Slice Description  |
|-----------------|-----------------|--------|----------------------|--|
| $\mathcal{S}_1$ | 690             | 0.1046 | -0.0897              | <b>age:</b> adult<br><b>skin-color:</b> dark               |
| $\mathcal{S}_2$ | 591             | 0.0921 | -0.0773              | <b>skin-color:</b> dark<br><b>cloth.-color:</b> dark-color |
| $\mathcal{S}_3$ | 349             | 0.0896 | -0.0748              | <b>gender:</b> female<br><b>skin-color:</b> dark           |
| $\mathcal{S}_4$ | 766             | 0.0778 | -0.0630              | <b>skin-color:</b> dark<br><b>blurry:</b> false            |
| $\mathcal{S}_5$ | 997             | 0.0594 | -0.0446              | <b>skin-color:</b> dark                                    |

Table 8: Quantitative analysis of the top-5 weak slices for the SETR semantic segmentation model trained and evaluated on Cityscapes dataset.



| Slice No.       | $ \mathcal{S} $ | $FNR$  | Avg. Perf.<br>Degra. | Slice Description                            |
|-----------------|-----------------|--------|----------------------|--|
| $\mathcal{S}_1$ | 541             | 0.8663 | -0.222               | age: young                                   |
| $\mathcal{S}_2$ | 510             | 0.8723 | -0.228               | age: young<br>construction-worker: false     |
| $\mathcal{S}_3$ | 405             | 0.8819 | -0.2376              | skin-color: dark<br>cloth.-color: dark-color |
| $\mathcal{S}_4$ | 349             | 0.9095 | -0.2652              | age: young<br>blurry: false                  |
| $\mathcal{S}_5$ | 173             | 1.00   | -0.4602              | age: young<br>skin-color: dark               |

Table 9: Quantitative analysis of the top-5 weak slices for the Panoptic-FCN model trained and evaluated on RailSem19 dataset. The cut-off threshold is reduced to  $1.0 * \bar{e}|\mathcal{S}|$  as  $\bar{e}|\mathcal{D}|$  is high in this experiment.